

~~The potentials~~Potentials of ~~high-resolution~~aerial and UAV photogrammetry for analyzing glacier retreat in the Ötztal Alps, Austria

Joschka Geissler^{1,4}, Christoph Mayer², Juilson Jubanski¹, Ulrich Münzer³ & Florian Siegert¹

5 ¹3D Reality Maps GmbH, Dingolfinger Str. 9, Munich, 81673, Germany

²Bavarian Academy of Science, Geodesy and Glaciology, Alfons-Goppel Str. 11, Munich, 80539, Germany

³Ludwig-Maximilians-University, Department of Earth and Environmental Sciences, Section Geology (remote sensing), Luisenstr. 37, 80333 Munich, Germany

10 ⁴Faculty of Environment and Natural Sciences, Albert-Ludwigs University Freiburg, Friedrichstr.39, 79098 Freiburg, Germany

Correspondence to: Florian Siegert (Siegert@realitymaps.de)

Abstract. ~~Glaciers all over the world experience an increasing mass loss during recent decades due to change in the global climate. This leads to considerable environmental consequences in the densely populated Alps and many other mountain ranges in the world. We used~~We use high-resolution aerial photogrammetry within the
15 ~~AlpSenseBench project to investigate glacier retreat in great spatial and temporal detail in the Ötztaler~~Ötztal Alps, a ~~significant glaeier~~heavily glacierized area in Austria. Long-term in situ glaciological observations are available for this region, and a multitemporal time series of digital aerial images with a spatial resolution of ~~20 cm~~0.2 m acquired over a period of ~~40 years exists~~9 years. ~~Digital surface models (DSMs) are generated for the years 2009, 2015, and 2018. Using these, glacier~~ retreat, extent, and surface elevation changes of all ~~2523~~ glaciers
20 in the region, including the Vernagtferner, ~~was are~~ analyzed ~~by investigating glacier extent and surface elevation changes, derived from the aerial images by digital surface model (DSM) generation.~~ Due to different acquisition dates of the large-scale photogrammetric surveys and the glaciological data, a correction ~~was established~~is successfully applied using a dedicated unmanned aerial vehicle (UAV) survey across the major part of the Vernagtferner. ~~This allowed us to compare~~The correction allows a comparison of the mass balances from geodetic
25 and glaciological techniques, ~~which reveals the potentials of the combination of these two techniques for gaining a better insight into glacier changes – both quantitatively and its spatial distribution spatially.~~ The results show a clear increase ~~of in~~ glacier mass loss for all glaciers in the region, including the Vernagtferner, over the last decade. ~~Additionally,~~Local deviations and processes, such as the influence of debris-cover on mass balance, ~~as well as dead-ice bodies, and~~ the magnitude of dynamic processes, ~~could be are~~ quantified. ~~The comparison of geodetic elevation differences and the interpolated glaciological data reveals that there exists a high potential in detecting~~Since those local peculiarities of mass balance distribution and for correcting small scale deviations, ~~processes are not revealed in the interpolated glaciological information captured with the glaciologic method, they underline the benefits of complementary geodetic surveying.~~ The availability of high-resolution multi-temporal digital aerial imagery for most of the glaciers in the Alps will provide a more comprehensive and
35 detailed analysis of climate change-induced glacier retreat.

1 Introduction

The impacts of climate change are widespread and clearly visible in the Alps (Rogora et al., 2018) but particularly evident in the dwindling glacier resources (Beniston et al., 2018; Sommer et al., 2020; Zekollari et al., 2019). Over the past 100 years, the temperature in the [European Alps, hereafter referred to as the Alps](#), has increased almost twice as fast compared to the global average, resulting in nearly 2 °C higher mean air temperatures (Auer et al., 2007; Marty and Meister, 2012). By the end of this century, mean air temperatures are expected to [rise](#) further [rise](#) by several degrees Celsius (Gobiet et al., 2014; Hanzer et al., 2018). Due to this ongoing climate evolution, alpine glaciers may lose half of their volume by 2050 compared to 2017 (Zekollari et al., 2019). The response of glaciers to climatic variations is directly related to the mass and energy balance at the glacier surface. Internal deformation and basal sliding redistribute ice from regions with mass gain (accumulation) to regions with mass loss (ablation), compensating the local imbalance with some lag in the response. [Changes in](#) [However](#), glacier geometry, [however](#), [changes](#) can be directly related to the mass balance if integrated across the entire glacier. Thus, the geodetic, glacier mean mass change (considering a volume to mass conversion) can be directly compared to glaciological mass balance measurements, based on local ablation and accumulation data.

We focused on a study site within the [Ötztal](#) [Ötztal](#) Alps, Austria, including the Vernagtferner, one of the reference glaciers in the World Glacier Monitoring Service (WGMS) system. Mass-balances have been determined here using the glaciological method since 1965, while a series of historical maps back to 1889 demonstrates the long-term glacier evolution over more than a century (Escher-Vetter et al., 2009).

~~Digital photogrammetry has been established as the standard method for cadastral surveys during the first decade of the new millennium. It is also used by BEV (Bundesamt für Eich- und Vermessungswesen, Austria) for their periodical digital elevation updates. Consequently, an immense imagery database has been generated, which allows three-dimensional reconstruction and mapping of vast areas in the Alps with a resolution in the order of decimeters. horizontal and vertical changes can be detected and analyzed on a large scale and with unmatched precision. Combining high-resolution photogrammetry with the extensive knowledge data base for the Vernagtferner acquired over more than a century, this study presents a unique combination of methods that allows the extraction of relevant glaciological information (glacier retreat and mass balances) with greater accuracy from aerial imagery. Data suitable for photogrammetric processing were available in three epochs over a period of 9 years (2009, 2015, 2018), and appropriate in-situ observations were used to evaluate and improve the remote sensing information.~~

~~The workflow was applied for all 25 glaciers within the study area, including the Vernagtferner. Past studies already~~ Along with Airborne Laser Scanning, digital photogrammetry is one of the standard methods for deriving geodetic glacier mass balances. Both methods have their weakness and strengths that were intensely analyzed and discussed within the scientific community (e.g., Baltasvias et al., 2001). ~~However, an undisputed and important advantage of the photogrammetric approach are the existing long-time series dating back into the last century. Past studies have used these time series to determine mass balances~~ (Belart et al., 2019; Jaenicke et al., 2006; Magnússon et al., 2016; Mayer et al., 2017). ~~Other studies~~ demonstrated the potential of spatiotemporal change analysis of alpine glaciers using photogrammetric data (Fugazza et al., 2018; Gudmundsson and Bauder, 1999; Legat et al., 2016; Rossini et al., 2018). ~~Though and also comparing their results to glaciologic data~~ (Baltasvias et al., 2001; Klug et al., 2018). ~~However~~, geodetic mass balances from photogrammetry are often restricted by

acquisition times and, therefore, not comparable with fixed date glaciological measurements (Fischer, 2011). ~~In this,~~

~~This study, aims at deriving geodetic glacier mass balances using high-resolution photogrammetric datasets provided by the Austrian Bundesamt für Eich- und Vermessungswesen (BEV) and 3D RealityMaps GmbH for 23~~

80 ~~glaciers within the Ötztal Alps, including the Vernagtferner. We processed photogrammetric data from airborne surveys for 2009, 2015, and 2018, thus covering a correction due to period of 9 years. This study presents, to our knowledge, a unique approach to correct~~ differences in acquisition dates between photogrammetric and glaciological data. ~~This~~ is achieved by employing an additional unmanned aerial vehicle (UAV) survey ~~and incorporating meteorological information~~. This calibration allows a parametrization between photogrammetry and
85 glaciology, revealing further potentials for these two techniques for accessing a more accurate insight into glacial retreat.

2 Study Area

90 ~~The Ötztaler Alpen~~Ötztal Alps are located in the central-eastern Alps and represent one of ~~the Austria's~~ most extensive glaciated regions ~~of Austria. The study area ranges from an, covering a range in~~ altitude of ~~1.700~~
~~mbetween 1700 to 3.768 meter~~3768 meters above sea level (m.a.s.l.) and ~~covers an area of~~ more than 250 km²

(Fig. 1). It combines the upper regions of the drainage basins of Rofental, Pitztal, and Kaunertal. The location in the inner part of the Alps leads to relatively low precipitation amounts (Fliri, 1975), which for example, reach

95 mean values of 660 mm yr⁻¹ at the valley station Vent in 1969-2006 (Abermann et al., 2009). For some of the ~~2523~~
glaciers within the study site ~~exist periods of, glaciologic~~ mass balance measurements ~~exist~~. One of the longest series of measurements ~~is can be found~~ at the Vernagtferner, where regular monitoring by the Bavarian Academy

of Sciences and Humanities (BAwH) began in 1965 (Escher-Vetter et al., 2009). This glacier is characterized by several sub-basins, which were connected to a single glacier tongue in former times. ~~Today~~In 2018, the glacier

100 ~~covers an area of covered~~ almost 7 km² within an altitude range between 2860 m.a.s.l. and 3570 m.a.s.l. The mass balance is determined by the glaciological method, using measurements at ablation stakes, manual and geophysical

depth soundings, and retrieving information from snow and firn pits. The annual and winter mass balances are determined independently of each other by measurements on the fixed dates of ~~1~~ May ~~1st~~ and ~~30~~ September ~~30th~~,

the dates of the glaciological balance year (Cogley, 2010; Cogley et al., 2011). Besides, there is a long history of
105 geodetic mapping at the Vernagtferner dating back to 1889 (Mayer et al., 2013a).

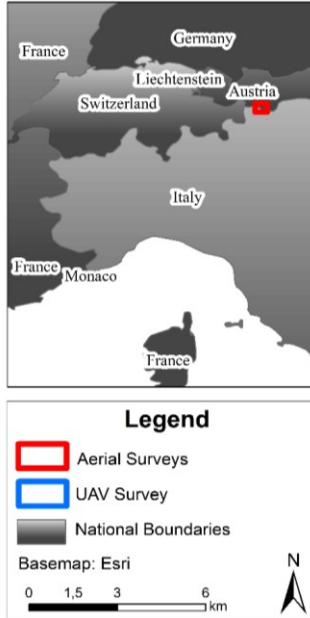


Figure 1: Study site in the Ötztal Alps; Red: area covered by aerial surveys; Blue: area of the Vernagtferner covered by the UAV Survey; Image source: ESRI (2020)

110 3 Data Acquisition

3.1 Photogrammetric data acquisition

After the introduction of the first large format digital aerial photogrammetric camera in 2000, this type of sensor quickly became the standard equipment for aerial surveys. The replacement of analog to digital equipment not only dramatically reduced the surveying costs, but also enabled the development of advanced three dimensional high resolution reconstruction algorithms based on photogrammetry. This kind of reconstruction works best with horizontal overlaps of more than 80%. Digital sensors allow surveys with this overlap because the high costs for photographic negatives no longer exist. Since the late 2000s, European state surveying agencies have been carrying out cadastral surveys every two to four years with digital sensors and horizontal overlap of 80%, thus creating an immense multitemporal database of aerial imagery to be explored both commercially and scientifically.

In Austria, cadastral aerial surveys are conducted by the BEV with a nominal resolution of 20 cm. We use a BEV survey from 2015 as a basis for our investigations. Besides, surveys performed by 3D RealityMaps in 2009 and 2018 with the same or higher ground resolution are investigated. Table 1 shows the most relevant information on the conducted air surveys.

In addition to the airplane-based surveys, a smaller test site was covered by an UAV flight to retrieve high-resolution data at another acquisition date closer to the maximum of ablation in 2018 (Table 1). The processed area covers 6 km² containing most of the glacier area of the Vernagtferner, including all glacier tongues. The glacier was almost snow-free at the time of the acquisition, which provides optimal processing conditions.

Table 1: Overview of the aerial data acquisitions

Date	Platform	Area [km ²]	Overlap (forward:lateral) [%]	Resolution [cm]	Images [Count]	Image type	Camera
09.09.2009	Airplane	257 km ²	80:40	20 cm	381	TIF RGB 8bit	UltraCam XP
03.08.2015	Airplane	330 km ²	80:50	20 cm	572	TIF RGBI 16bit	UltraCam XP
21.09.2018	Airplane	260 km ²	80:60	20 cm	428	TIF RGBI 16bit	UltraCam Eagle Mark 2
21.08.2018	UAV	6 km ²	80:80	5 cm	1992	JPEG RGB 8bit	UMC-R10C

Formatierte Tabelle

3.2 Glaciological mass balance data acquisition

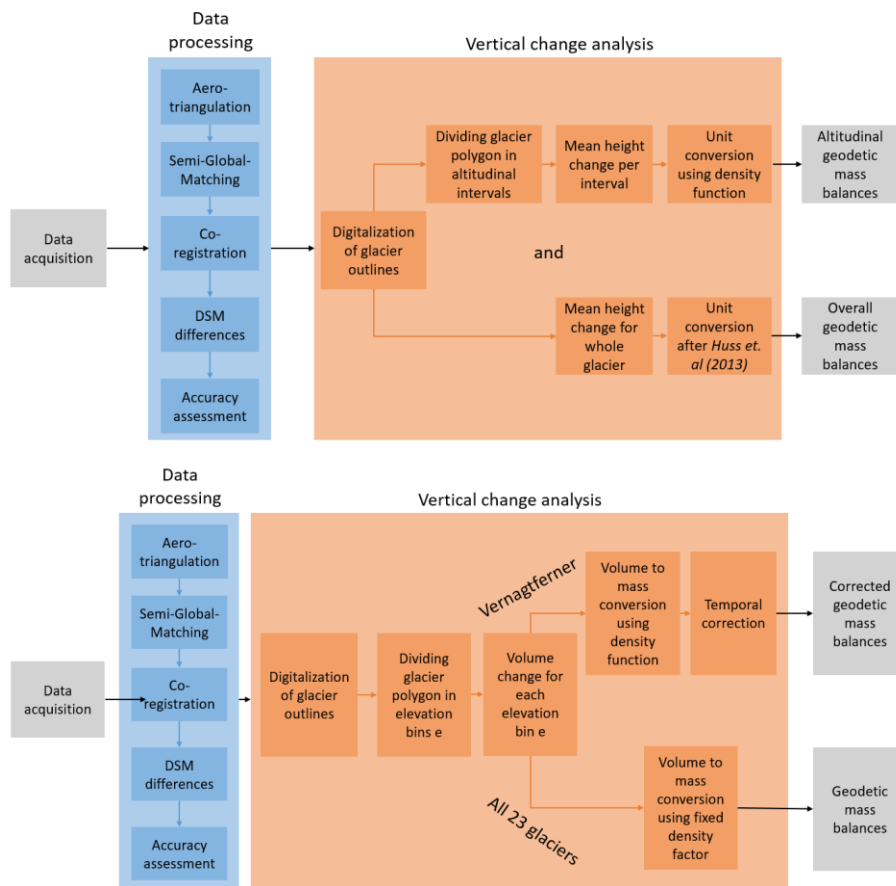
Glaciological mass balance data are acquired at the Vernagtferner since 1965. Information is gathered as stake readings from ablation stakes for estimating the ice melt across the glacier. At the same time, snow depth and last season firn deposits are determined from mechanical depth soundings with metal probes, which are then combined with density information from snow and firn pits to calculate the ice-water equivalent of the remaining snow and firn cover. While stake readings only require two length measurements per stake with an

uncertainty of typically about 1 cm, more significant errors are included in the direct accumulation measurements due to uncertainties in the sample volume (about 5%) and the determination of density by using spring scales (about 4%). Therefore water equivalent accuracy is about 6% (Zemp et al., 2013). The typical number of stakes used for the annual mass balance measurements at the Vernagtferner is about 35, while ~~some~~ 4-5 accumulation measurements are collected at the end of the glaciological year, ~~30 September~~ 30th. The equilibrium line, which represents a mass balance of zero, is derived by comparing oblique terrestrial photographs of the transient snow line and firn extent with optical remote sensing information close to the ~~date of the field measurements~~ measurements' date. The derived equilibrium line has a horizontal location accuracy of about 10 m. Glacier boundaries for delineating the spatial mass balance distribution are derived from aerial surveys repeated roughly ~~each~~ every decade, ~~which are~~ updated in the ablation region by annual GNSS (Global Navigation System Services) measurements of the glacier tongue geometry. The spatial error of these measurements is usually better than 1 m. The information from the stake readings, the depth soundings, the snow ~~and firn~~ pits, and the location of the equilibrium line are combined to interpolate the spatial distribution of the glacier mass balance into a raster file. Due to the sparse information in the accumulation region, it is necessary to manually correct the interpolation results in this region ~~by~~ with the knowledge of the long-term accumulation patterns, which are rather persistent. Errors introduced by uncertainties in the accumulation region, however, are ~~rather~~ relatively small, especially during the recent decade where the accumulation area ratio is usually well below 30%. While ablation varies between 0 and up to ~~4500 mm~~ 4.5 m w.e. a⁻¹ in the ablation area, accumulation only varies between 0 and about ~~300-400 mm~~ 0.3-0.4 m w.e. a⁻¹ in the accumulation area. Within this study, we assumed the error of the interpolated ~~glaciologic~~ raster to be ~~100 mm~~ 0.1 m. w.e. a⁻¹, which is in accordance ~~to~~ with Zemp et al. (2013). It must be noted, that this relatively large error within the accumulation area will only affect the final mass balance by less than 2 %.

4 Methods

4.1 Photogrammetric workflow

~~In order to~~ To determine geodetic glacier mass balances from aerial and UAV images, we ~~use~~ used a workflow consisting of two main modules: the data processing (sect. 4.1.1) and the vertical change analysis (sect 4.1.2; Fig. 3). The main goal of the data processing module ~~is~~ was the reconstruction from raw imagery data into 3D point clouds. Digital surface models (DSM) and true orthophoto mosaics (TOM) ~~are~~ were then derived from these point clouds. Finally, DSM differences ~~are~~ were computed. Within the vertical change analysis module, geodetic glacier mass balances ~~are~~ were computed from the DSM differences.



170 **Figure 2: Full photogrammetric workflow; Blue: From raw images to DSM differences; Orange: From DSM differences to overall and altitudinal mass balances**

4.1.1 Data processing

175 The first step in data processing *is* was the aerotriangulation, which consists of the orientation of the aerial imagery to the real terrain. Modern photogrammetric survey systems deliver highly accurate *position* (*positions using* GNSS) and orientation (IMU, inertial measurement unit) information for each image, which *are* were also included in the aerotriangulation for the georeferencing. Finally, at least 20 tie points were manually identified for each image block to enhance the orientation accuracy. For the large format imagery, the aerotriangulation was performed using the *state-of-art* software *Match-AT* by Trimble. For the UAV imagery, the software *Metashape*
 180 *Professional* from Agisoft was used.

The second stage of data processing ~~is was~~ the generation of point clouds through three-dimensional reconstruction. For this purpose, the state-of-the-art Semi-global-matching algorithm (Heipke, 2017; Hirschmüller, 2019) was used. This algorithm ~~is was~~ implemented within the software *SURE* (nFrames), which generates DSM and TOM from the point clouds. ~~Positioning accuracies~~The horizontal shift of the derived TOM and DSM ~~were was~~ computed

185 based on ground control points from the BEV. ~~The horizontal shift and~~ lies between 10 and 20 cm depending on the acquisition year and thus within the ground resolution of the images.

~~In order~~Due to calculate these excellent values, only a vertical co-registration of the DSM differences was applied. ~~Therefore,~~ existing systematic height shifts ~~between all DSMs~~ were ~~corrected by~~ derived using 50 stable areas (mostly large points (e.g., solid rock formations) outside the glaciers. ~~21 stable points were used for the UAV-~~

190 ~~survey.~~ The 2015 DSM was chosen as the reference because it was derived from the official Austrian cadastral survey and is referenced to the Austrian national survey system. ~~The mean shift in elevation compared to the reference DSM was computed based on 50 identified stable points, e.g., on solid rocks, for each DSM and 21 stable points for the UAV-survey.~~ Based on this mean vertical shift over stable ground, all DSMs except for the reference DSM were adjusted in height relative to the reference DSM of 2015. Subsequently, the DSM differences

195 9/2018–8/2015, 8/2015–9/2009, 9/2018–9/2009, and 9/2018–8/2018 were computed and named after their acquisition dates.

4.1.2 Vertical change analysis

~~For~~The goal of the vertical change analysis (Fig. 2, orange part), ~~glacier outlines were digitized visually using the TOMs at a scale of 1:2.000. The geodetic glacier mass balance (B) for a single glacier is determined by-~~ was to

200 ~~quantify elevation changes Δh_t within our study area from the DSM differences of different time periods t. By integrating the DSM difference Δh_t over the glacier outline a specific area S_t , volume change ΔV was determined by the following equation, where r is the pixel size (Fischer, 2011; Zemp et al., 2013):~~

$$\Delta V_t = r^2 * \int_0^{S_t} \Delta h_t \quad (1)$$

~~To derive overall geodetic glacier mass balances $B_{\text{geod},t}$, ΔV_t was determined with S_t being the area at the beginning of the respective period. The result is divided by the mean glacier area of the period. More details can be found, for instance, in -~~ For the t (Fischer, 2011), S_t was digitized visually using TOMs at a scale of 1:2.000. For the following volume to mass conversion in mm water equivalent (w.e.), we used the density assumption proposed by Huss, (2013) ($\bar{\rho} = 850 \text{ kg m}^{-3} \pm 60 \text{ kg m}^{-3}$; was used. To determine) for all glaciers.

$$B_{\text{geod},t} = \frac{\Delta V}{S} * \frac{\bar{\rho}}{\rho_{\text{water}}} \quad \text{with} \quad \bar{S} = \frac{S_{t=\text{begin}} + S_{t=\text{end}}}{2} \quad (2)$$

~~To allow a detailed analysis of the altitudinal dependencies of the glacier mass balances, the glacier polygons were area was divided into 10 m altitudinal intervals additionally elevation bins c. For each altitudinal interval bin,~~

210 the mean absolute height change in meters was determined as well. For geodetic mass balance $B_{\text{geod},e,t}$ was derived with the conversion in mm w.e., an altitude-related density functions was used. Its same equations (see Eq. 1, 2 and Zemp et al. (2013)).

~~For the Vernagtferner, the altitude of the equilibrium line altitude (ELA) is known from intense glaciologic surveys on an annual basis (BAdW, 2019). It lies at 3217 m.a.s.l. for the period 2009-2015, 3278 m.a.s.l. for the period~~

215 ~~2015–2018 and 3237 m.a.s.l. for 2009–2018. Thus, we were able to use an altitude-related density function $\bar{\rho} = f_{t,d}(e)$ for converting surface changes to mass relative to the altitude of the ELA. This density function $f_{t,d}(e)$ [kg~~

m^{-3}) represents the gradual change from ice density (900 kg m^{-3}) in the ablation region to firn density (550 kg m^{-3}) (Cogley et al., 2011) in the accumulation region with elevation e, by using a linear transition zone of $\pm 50 \text{ m}$ across around the equilibrium line altitude (ELA) of the respective period t:

$$f_{t,d}(e) = \begin{cases} 550 & \text{for } e > \text{ELA} + 50 \text{ m} \\ 725 - 3.5 * (e - \text{ELA}_t) & \text{for } e \text{ between } \text{ELA} \pm 50 \text{ m} \\ 900 & \text{for } e < \text{ELA} - 50 \text{ m} \end{cases} \quad (3)$$

220 **4.2 Comparison with glaciological data**

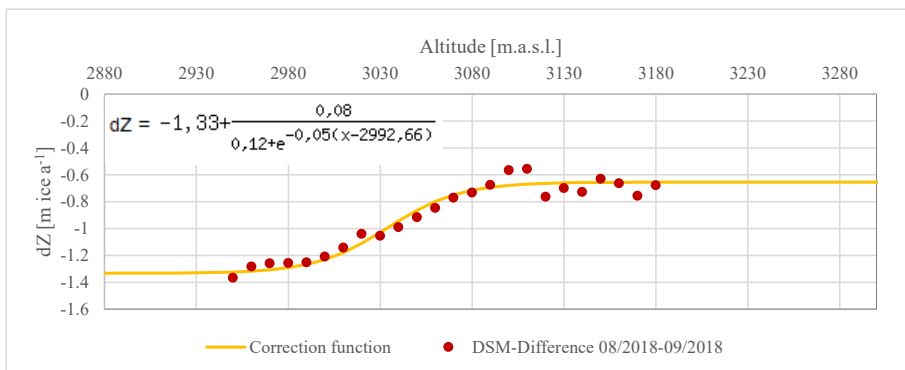
To be able to compare the mass balances determined glaciologically and photogrammetrically, they must have the same period. For this purpose, the annually available To allow a comparison of both, the geodetic and glaciologic mass balances, annual glaciological mass balances were accumulated to the periods 09/2009-09/2015, 09/2015-09/2018, and 09/2009-09/2018. The acquisition dates and reanalyzed according to the Steps 1 to 4 in Zemp et al. (2013). Thus, mean annual mass balances of the respective periods were derived as well as systematic and random errors (sect. 3.2, 4.3 photogrammetric data differ from the glaciological measurements (-). To account) for the all geodetic datasets following Nuth and Kääb (2011) (Sect. 4.3). Because one main objective of this paper was to analyze systematic differences between the two methods, iterative adjustment and calibration of the data (Step 5-6, Zemp et al. (2013)) was not performed.

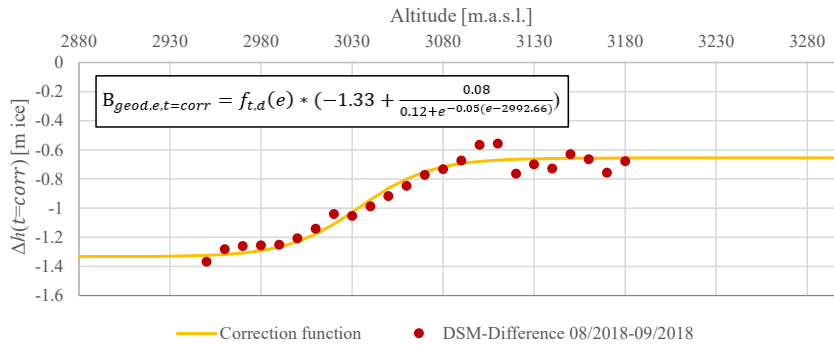
225 The remaining temporal differences, which are limited to the period of maximum ablation in August and September, the between the photogrammetric and glaciologic acquisition times were addressed using an additional photogrammetric DSM difference. A regression (sigmoid, see Fig. 3-) was performed for deriving the surface elevation change $\Delta h_{k,t=corr}$ (Table 2). By multiplying $\Delta h_{t=corr}$ with the altitude related density assumption $f_{t,d}(e)$ (Eq. 3) the mass balance $B_{geod,e,t=corr}$ for all elevation bins e and the correction period $t=corr$ (08/2018-09/2018) was used. From this, a correction function (sigmoid, see -) was derived. For the regression, only Only those altitude levels were considered for the regression, which were at least 40- % covered by the UAV survey. The standard deviation (SD) of the regression is 0.07 m ice- a^{-1} (Fig. 3). Above 3180 m.a.s.l., thus, for the accumulation areas, the correction function is not based on any data and is therefore error-prone. Additionally, for the correction of the time periods, it had to be assumed that the ablation process was constant during the period between August 21st and September 21st, 2018, and that the magnitude was comparable to the years of 2009 and 2015.

230

235

240





245 **Figure 3: DSM difference Surface changes in 10 m altitude bandsbins for the period 08/2018–09/2018 (red dots); Correction function Regression curve (yellow) for acquisition date correction_t, representing height changes related to the altitude within one month in August and September 2018; SD of the regression is 0.07 m ice a⁻¹.**

250 Subsequently, the DSM differences were adjusted according to the number of days the investigation periods differ using a correction factor, and the correction function (-). The correction factor converts the number of deviating days into months, thus represents the factor of which the monthly ablation (correction function) is added to the respective DSM difference.

Table : Correction of photogrammetric DSM differences due to differences in acquisition dates; The Correction factor is computed by dividing the number of days that deviate through 30 days per month.

255 To transfer this information to other time periods, we used temperature time series measured at a climate station close to the Vernagtferner at 2640 m.a.s.l.. Positive Degree Day Sums (PDD_{e,t}) [°C] were computed for all elevation bins e and time periods t, the geodetic and glaciologic method needed a correction for (Table 2). For this step, we assumed the vertical lapse rate of the air temperature to be -0.6 °C per 100 meters of altitude. This allowed the Degree Day Function (DDF) to be determined for all elevation bins e (Eq. 4). More information on this method
260 can be found, for instance, in Braithwaite and Zhang (2000) and Hock (2003).

DSM-difference	Acquisition-date photogrammetric-data	Acquisition-date glaciological-data	Deviation Number of days {days}	Correction Factor {months}
09/2009–08/2015	09.09.2009	03.08.2015	30 th of September each year	+1,2
08/2015–9/2018	03.08.2015	21.09.2018	30 th of September each year	-1,6
09/2009–09/2018	09.09.2009	21.09.2018	30 th of September each year	-1,2
				-0,(4)

Gelöschte Zellen

Gelöschte Zellen

Gelöschte Zellen

Gelöschte Zellen

Formatiert: Vom nächsten Absatz trennen, Diesen Absatz nicht zusammenhalten, Position: Horizontal: Links, Gemessen von: Spalte, Vertikal: Normalfolge, Gemessen von: Seitenrand, Horizontal: 0 cm, Umschließen

Formatierte Tabelle

Formatiert: Rechts, Vom nächsten Absatz trennen, Diesen Absatz nicht zusammenhalten, Position: Horizontal: Links, Gemessen von: Spalte, Vertikal: Normalfolge, Gemessen von: Seitenrand, Horizontal: 0 cm, Umschließen

hat formatiert: Schriftart: Cambria Math, Kursiv

The geodetic mass balance for the correction periods $B_{e,t}$ could then be determined for the time periods t of length d_t and in all elevation bins e :

$$B_{geod,e,t} = DDF_e * PDD_{e,t} * d_t \quad (5)$$

Subsequently, for the density conversion of the adjusted the DSM differences $B_{geod,e,09/2009-2018,2009-08/2015}$ and $B_{geod,e,08/2015-09/2018}$ and $B_{geod,e,09/2009-09/2018}$, the altitude related density assumption (ρ) was used. Finally, were corrected according to Table 2.

Table 2: Correction parameters (left) of all correction periods t and the adjusted DSM differences were subtracted from the corresponding applied corrections to all geodetic mass balances (right).

t	Acquisition date photogrammetric data		d_t [days]	$PDD_{e=2870\text{ m.a.s.l.},t}$ [°C]	Applied Corrections
1	09.09.2009	30.09.2009	21	82.45	$B_{geod,e,09-15} = B_{geod,e,09/2009-08/2015} - B_{geod,e,t=1} + B_{geod,e,t=2}$
2	03.08.2015	30.08.2015	27	280.76	$B_{geod,e,15-18} = B_{geod,e,08/2015-09/2018} - B_{geod,e,t=2} + B_{geod,e,t=3}$
3	21.09.2018	30.09.2018	9	46.58	$B_{geod,e,09-18} = B_{geod,e,09/2009-09/2018} - B_{geod,e,t=1} + B_{geod,e,t=3}$
corr	21.08.2018	21.09.2018	3	176.81	

The overall geodetic mass balances $B_{geod,t}$ of the Vernagtferner was then derived from the mass balances of the single elevation bins e and their respective area $S_{e,t}$ (Zemp et al., 2013):

$$B_{geod,t} = \frac{\sum_{e=1}^E B_{geod,e,t} * S_{e,t}}{S_t} \quad (6)$$

Finally, accumulated glaciologically derived rasters $B_{glac,t}$ (sect. 3.2-) were subtracted from the adjusted geodetic mass balances $B_{geod,t}$. The resulting Variation Rasters Var_t show the spatial deviations between the two methods:

$$Var_t = B_{geod,t} - B_{glac,t} \quad (7)$$

Using this Variation Raster, local methodical we analyzed spatial deviations (e.g. between both methods that occur due to differences in the individual methods and related errors (e.g., neither including the supra-glacial debris cover or crevassed areas) were quantified, for surface ablation nor dynamic processes within the glaciologic method). Therefore, the respective areas were manually we digitized, and the respective areas on the Vernagtferner by using the geodetically derived TOMs of 2009 and 2018 and computed the mean value of variation (difference between the geodetic and the glaciologic mass balances) by using the Variation Raster was calculated. This value can be related to the total mass balance to estimate (Eq. 7) as well as Eq. 1 and 2. By comparing this mean variation with the mean variation of areas within the same elevation bin, we estimated the magnitude of methodological error introduced by neglecting those areas within glaciological mass balances.

4.3 Vertical accuracy assessment

To assess the error distribution within the study area after the coregistration, 1.5 km² of ice-free, stable terrain were analyzed, representing a wide range of slope, aspect, and altitude. Therefrom, the The mean shift as well as and the standard deviation SD within those areas was were calculated, and their relation to topography was investigated, following Nuth and Käab.

(2011). To estimate the error when averaging over extended areas, we followed Rolstad et al. (2009) by assessing the spatial covariance of the elevation differences with the use of using semivariograms. For the application of the

hat formatiert: Tiefgestellt
hat formatiert: Tiefgestellt
hat formatiert: Tiefgestellt
hat formatiert: Tiefgestellt

hat formatiert: Englisch (Vereinigte Staaten)
hat formatiert: Englisch (Vereinigte Staaten)
hat formatiert: Englisch (Vereinigte Staaten)
hat formatiert: Englisch (Australien)

method, we assumed that elevation ~~differences~~ differences are constant in space, ~~do not contain any~~ large-scale trends, and that there is no significant variation of the variance in space.

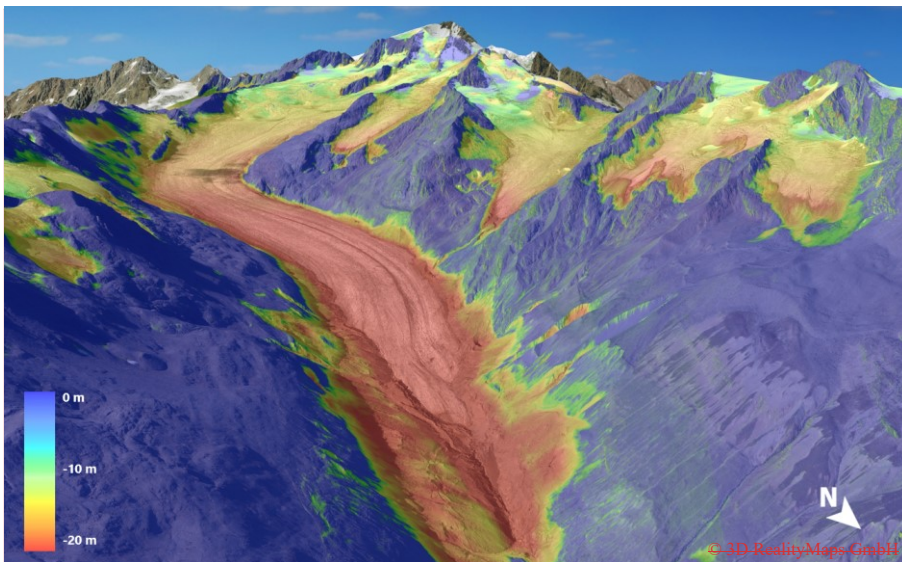
Basic error propagation was implemented (Nuth and Kääb, 2011; Zemp et al., 2013) ~~in order~~ to determine the compound error of DSM differences, density conversion (7 %, sect. 4.1.2, ~~Huss (2013)~~), the correction function of the acquisition dates (SD = 0.07 m ice a⁻¹, sect. 4.2) as well as the error associated to the glaciological interpolation raster (sect. 3.2) for all presented results. The error within this study is indicated by the 95% confidence interval.

5 Results

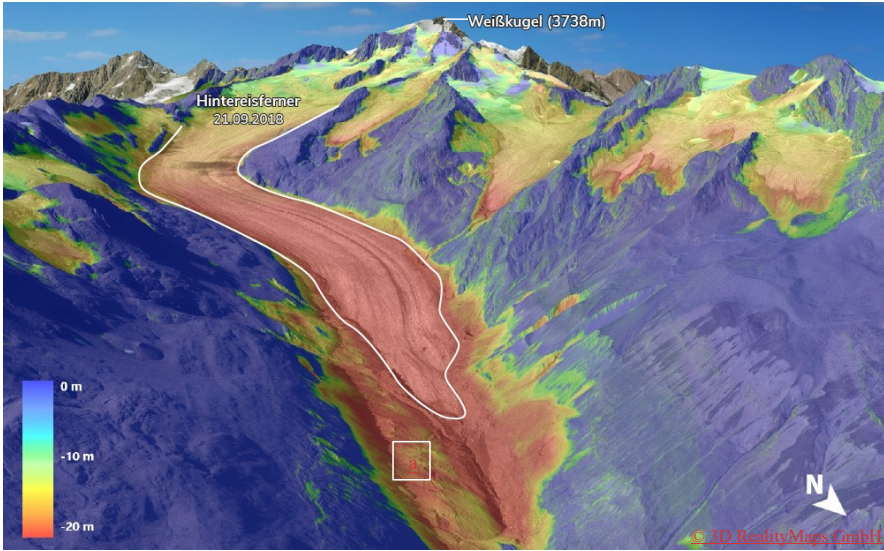
5.1 Vertical Change Analysis

5.1.1 Visual assessment

Using the ~~photogrammetrically~~ derived glacier outlines, TOMs, ~~as well as the~~ and DSM differences, the first results are obtained by a visual interpretation for the entire study area. In general, glaciers ~~were losing mass during the recent decade~~ have thinned and ~~thus are declining~~ reduced in terms of their size and ice thickness. For instance, ~~surface height changed at~~ the glacier tongue of the Hintereisferner ~~has lost more than by up to~~ -20.4 ± 0.4 m in height during the nine years from 09/2009 to 09/2018 (Fig. 4). With increasing altitude, the loss of height on the glacier approaches zero. ~~A dead ice body can be seen close to the glacier tongue (Fig. 4a)~~. Analyzing the TOM of the three surveys, reveals that the eastern part of the Hochjochferner lost a considerable area along its lower glacier margin. Especially its main tongue shortened, ~~not considering remaining dead ice bodies~~, by 826.4 ± 0.2 m between 2009 and 2018 (Fig. 5). ~~A further visualisation~~ Further visualization of this evolution ~~the DSM differences~~ can be assessed at <https://og.realitymaps.de/AlpSense/>.

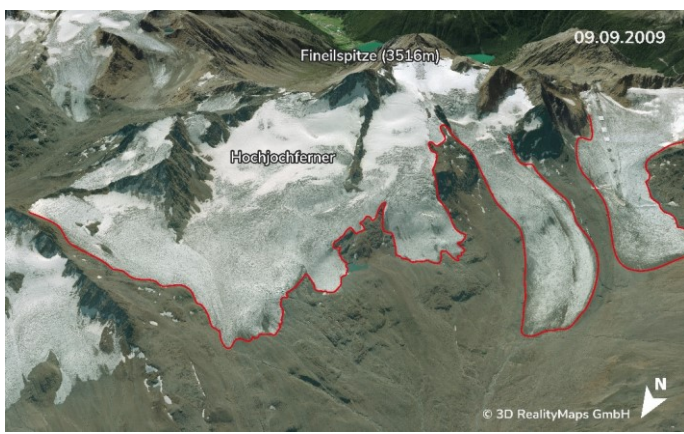
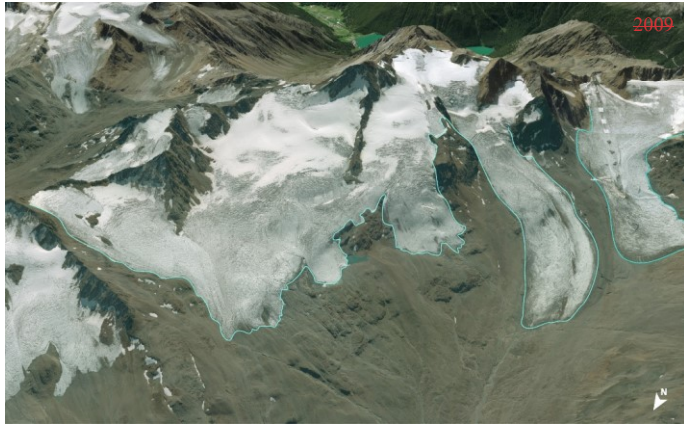


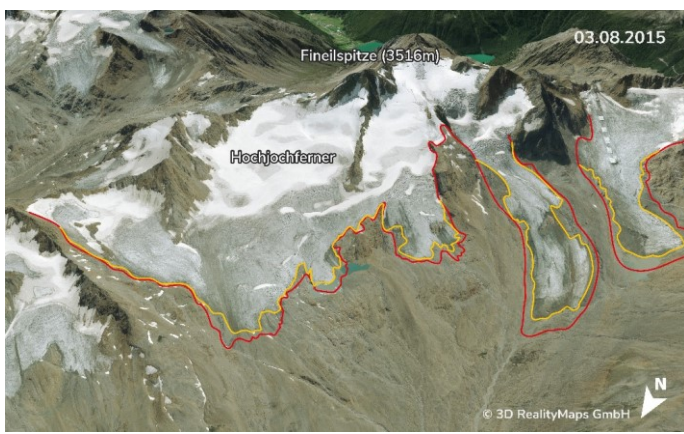
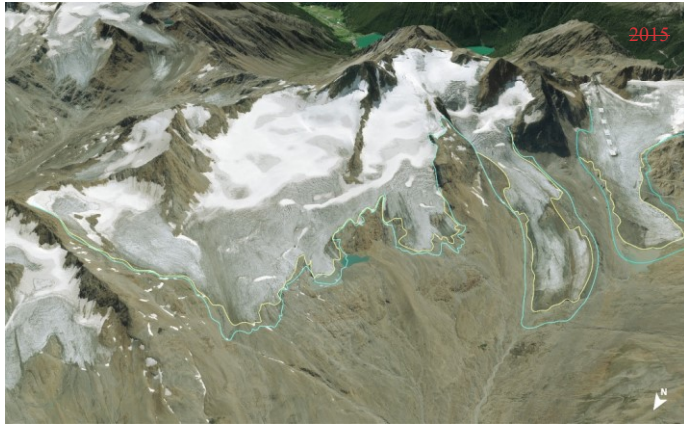
Kommentiert [JG1]: Gipfel benennen

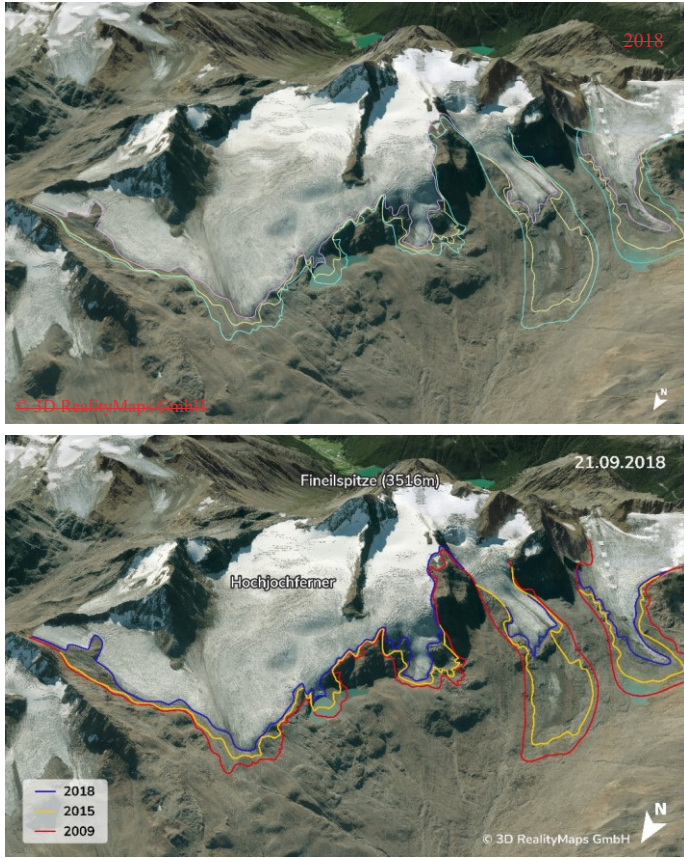


315 Figure 4: **Visual3D** representation of the height differences **in meter (m)** between the DSMs of 09/2009 and 09/2018 for Hintereisferner. **(white outline)**. **A dead ice body is visible south-east of the glacier tongue (a)**. Surface height differences are color-coded. Ice loss is especially high at altitudes below 2.500 m.

hat formatiert: Schriftart: Nicht Fett





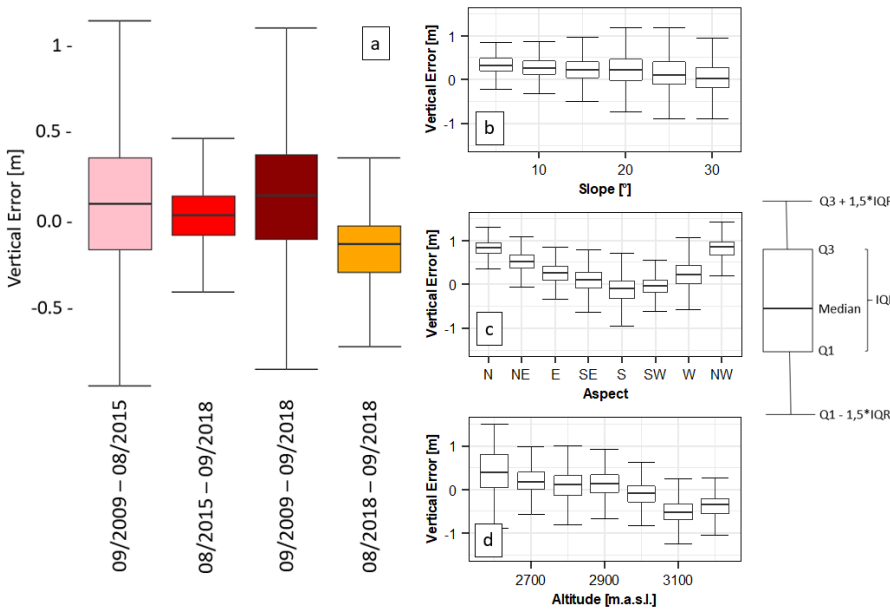
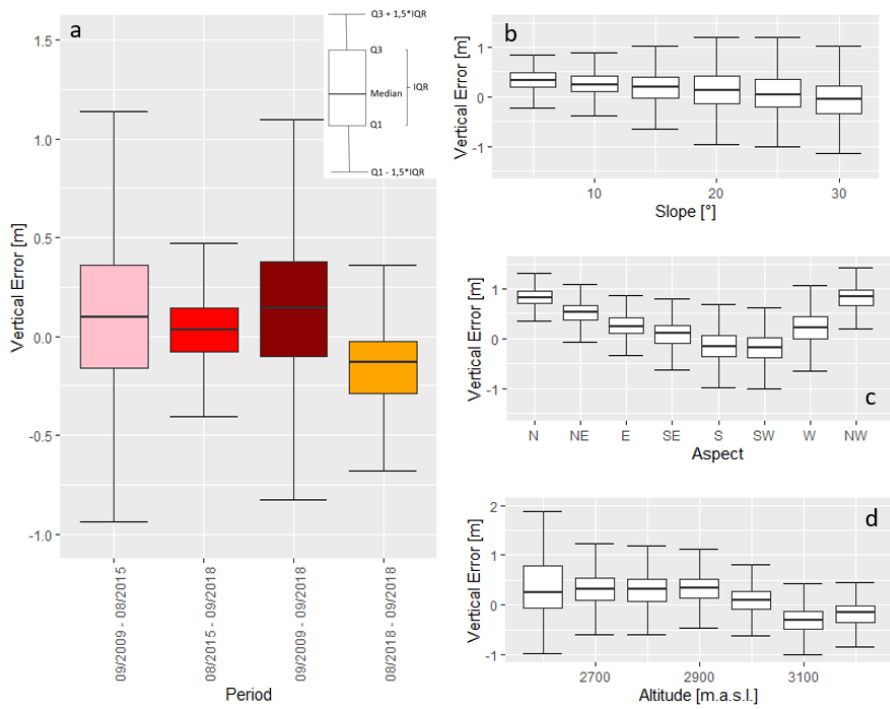


320 **Figure 5: Visual assessment 3D visualization of the length change for the Hochjochferner; in 2009 (top), 2015 (middle), and 2018 (bottom); Lines indicate glacier extent for the respective years. The glacier tongue in the center-right lost 826 m in 9 years.**

5.1.2 Vertical accuracy assessment

325 The accuracy assessment conducted (sect. 4.3) allows an estimation of potential error related to the DSM
differences and derived products. In general, the mean vertical error of the DSM differences ranges from -0.16 m
to 0.1 m with SD not exceeding 0.42 m (Fig. 6a). As expected, SD increases with the slope (Fig. 6b). ~~A clear~~
apparent increase of the SD can also be found in lower altitudes (< 2600 m.a.s.l., (Fig. 6d), most likely due to the
increasing influence of vegetation. A relation between aspect and the vertical error was found (Fig. 6c), ~~that~~
330 which can be attributed to the horizontal shift of the DSMs (see sect. 4.1.1) (Nuth and Kääh, 2011).

Based on the error assessment, the confidence interval for all results within this paper was determined. Therefore,
semivariograms were computed for the 1.5 km² bedrock areas for all observation periods, from which the range-
value (100 m) was conducted and converted to the correlated area value (31416 m²). For more detailed information
~~of~~
335 on this method, see Rolstad et al. (2009).



340 **Figure 6: Error assessment of the DSM differences in general (a) and in relation to topography (right); Boxplots in the right column have been plotted using the DSM difference 09/2009- 08/2015**

5.1.3 Mass balances

345 ~~Mass balance analysis was focussed on the Volumetric changes $\Delta V_{t,e}$ and height changes $\Delta h(t,e)$ for every elevation bin e were derived for all periods t and all glaciers, before and (for the Vernagtferner because only) after the correction of acquisition dates (Eq. 1 – 2, Fig. 7 data-availability. It must be considered that the height changes per altitude are not equal to the glaciological vertical balance profile of a glacier, because there are still contributions of firn processes and ice dynamics included in-).~~

350 ~~Before and after the temporal correction, the signal. However, the mean annual height changes per altitude elevation bin show a characteristic shape with height changes being the highest losses most negative at the glacier tongues and a large difference. The period between the investigation periods of 09/2009-08/ and 2015 and 08/ generally shows less negative values than the period 2015-09/ and 2018 (in all altitudes for all glaciers (Fig. 7, bottom). However, it needs to be considered that the investigated periods do not cover full mass-balance years, which influences the annual mean values considerably. Therefore height changes for left) and the Vernagtferner were corrected (as described in sect.) to scale the results to full mass-balance years (Fig. 7, top left). After the correction, there remains a the difference in height change between the two periods, albeit is considerably smaller. 355 The later period between 2015-2018 generally shows more negative values than during the period 2009-2015, which now also affects the highest~~

~~Compared to the height changes, the most negative volume change occurs in higher elevations of the glacier. Based on since it is linked to the area-height-distribution by altitude, the volume change per 10 m height interval can be calculated from the annual height changes of a glacier. After correcting for the acquisition dates, the elevation of maximum annual volume loss and its magnitude clearly increased between the investigation periods. Specifically, based on the regression curve (gaussian Gaussian fit) for the corrected values of the Vernagtferner, between 2009 and 2015, the most negative volume change of -0.21 ± 0.01 Millionmillion $m^3 a^{-1}$ was lost occurred at an altitude of 3009-3019 m.a.s.l. between 2009. Between 2015 and 2015, while 2018, the amount and altitude of the maximum most negative volume loss increased change further decreased to -0.29 ± 0.02 Millionmillion $m^3 a^{-1}$ at an increased altitude of 3089-3099 m.a.s.l. (Fig. 7, top right). The same trend was found for all glaciers within the study area, although no correction was applied to those values (Fig. 7 for 2015-2018 (-), bottom right).~~

360
365

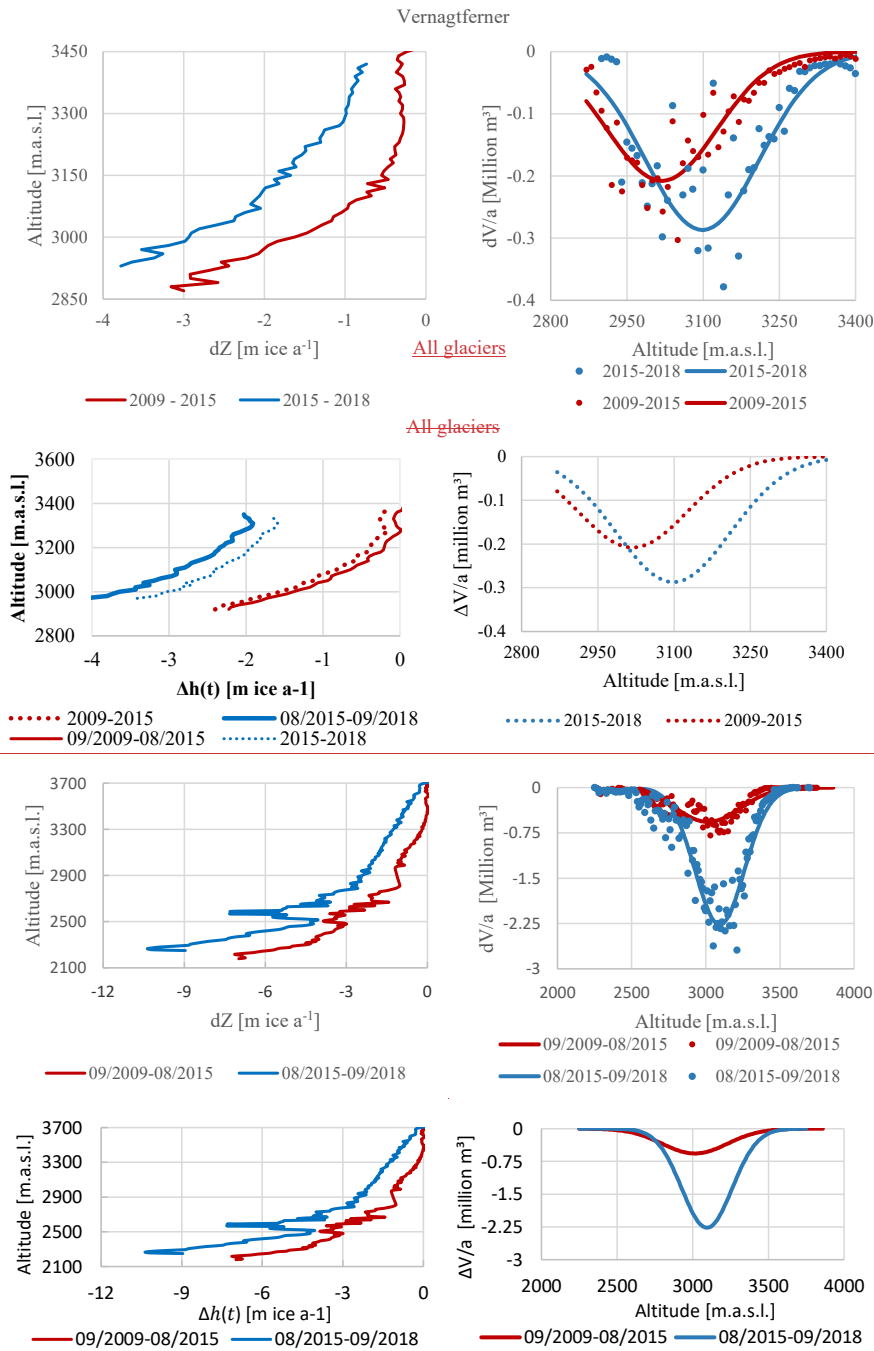


Figure 7: **Left**: Top left: Annual height changes $\Delta h(t)$ per altitude for the Vernagtferner (top) and, Bottom left: Surface height changes of all glaciers (bottom); **right**: Right: annual volume changes for the Vernagtferner (top) and all glaciers

(bottom); Values Dotted lines represent the surface or volume changes after the correction of the acquisition dates to glaciological balance years.

5.2 Comparison with glaciological measurements

The photogrammetric, as well as the geodetic and glaciological mass balances of the Vernagtferner, were further compared to detect discrepancies in spatial distribution or magnitude between both methods presented. Therefore, the DSM differences, as well as the overall geodetic mass balances, were compared to the equivalent accumulated glaciologically derived mass balances. At the same time, the correction of the acquisition dates is evaluated. As already noted, the overall mass balance for the Vernagtferner is more negative in the period 2015-2018 than in the period 2009-2015. This can be seen in both, the glaciological and the geodetic mass balances (Fig. 8). The uncorrected photogrammetric geodetic mass balance (blue) does not equal the corresponding glaciological mass balance (orange). After the correction of acquisition dates (red), the photogrammetrically derived geodetic mass balance has approached to the glaciological data. However, the corrected data is still lower more negative for the period 2015-2018 and higher for the period 2009-2015. This suggests, that the correction for the acquisition dates underestimated the melting processes. For the period 2009-2018, where the correction function has lowest impact due to i) a longer time period and ii) lowest number of deviating days (-), the 2015 corrected photogrammetric data lies within the error bars of the geodetic and glaciologic data mass balances match.

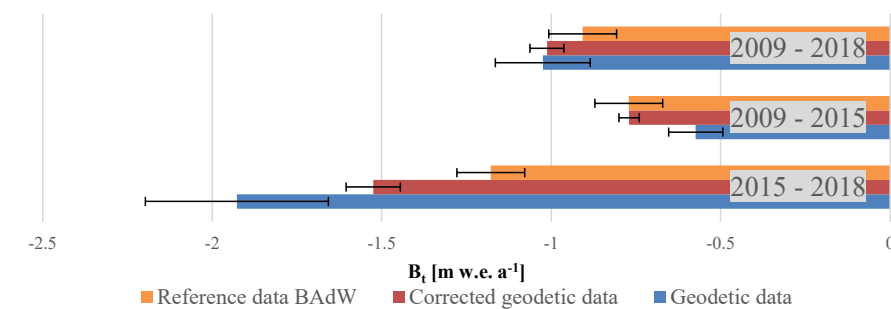
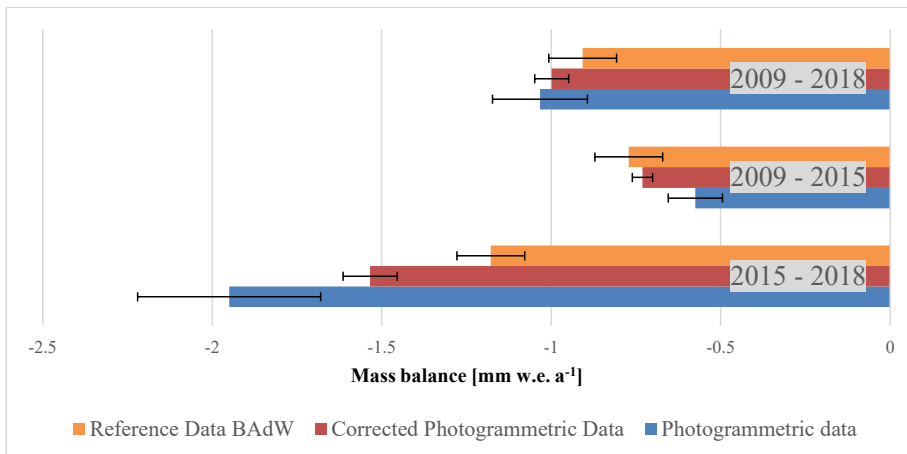


Figure 8: Comparison between **photogrammetriegodetic** mass balances (blue) and glaciological mass balances (orange) for the investigation periods. Red bars visualize corrected **photogrammetriegodetic** data.

395

The spatial differences between both methods were further investigated using the Variation Raster described in sect. 4.2. ~~The ... It is noticeable that the~~ Variation Raster ~~represents spatially distributed deviations of the interpolated rasters based on the glaciological field measurements from the corrected DSM differences based on photogrammetric data (sect. ,).~~

400 High spatial variations occur more positive (thus $B_{glac,t} < B_{geod,t}$, see Eq. 7) in debris-covered areas compared to its surrounding cells (red in Fig. 10), ~~where photogrammetrically derived mass balances are higher than glaciological mass balances.~~ Since no ablation stakes are located in supra-glacial debris at the Vernagtferner, ~~the~~ and glaciological mass balances ~~for these areas~~ are interpolated from surrounding information on clean ice, ~~the effect of debris is neglected within the glaciologic method.~~ Debris cover above a certain thickness protects the glacier against incoming heat fluxes (Östrem, 1959) and therefore reduces the ablation. ~~For the entire Vernagtferner, the neglect of debris-covered areas within glaciological interpolation lead to an underestimation of the glaciological mass balance by about $0.1 \text{ m} \pm 0.08 \text{ w.e. a}^{-1}$ ($0.8 \pm 0.6 \%$).~~ With our Variation Raster, we were able to quantify the effect of neglecting debris-covered areas within the glaciological interpolation: For 2018, a total area of 91350 m^2 (1.5 % of the total area of the Vernagtferner) at a mean altitude of 3040 m.a.s.l. was classified as debris cover. The variation between the geodetic and glaciologic method for those debris-covered areas is $5.02 \pm 0.89 \text{ m w.e. a}^{-1}$ and thus more positive than the mean variation at the respective altitude $0.38 \pm 0.27 \text{ m w.e. a}^{-1}$ (period 2009–2018, see Fig. 9). Considering the difference of those values, the overall glaciologic mass balance of 2009–2018 would be $0.07 \text{ m w.e. a}^{-1}$ (7.7 %) less negative if debris-covered areas were considered in the interpolation.

hat formatiert: Englisch (Australien)

415 Further analysis of the Variation Raster (Fig. 10) emphasizes that **photogrammetriegodetic** and **glaciologically derivedglaciologic** mass balances do not only differ ~~spatially~~ due to debris cover or other ~~external~~local effects. ~~More precisely, it is also~~ evident that the deviations depend on the altitude. Thus, in the lower reaches of the glacier, ~~photogrammetriethe geodetic mass balances are higherbalance is less negative~~ than the glaciological mass balances. For higher altitudes, ~~photogrammetriethe geodetic mass balances are lowerbalance more negative~~ than the glaciologically derived ones. This pattern is usually attributed to the ice dynamic component of elevation change contained in the geodetic differences (submergence and emergence of ice and firm). Additionally, Fig. 9 clearly shows that comparing the different observation periods, the bias between both methods becomes larger within the accumulation areas.

hat formatiert: Englisch (Australien)

425

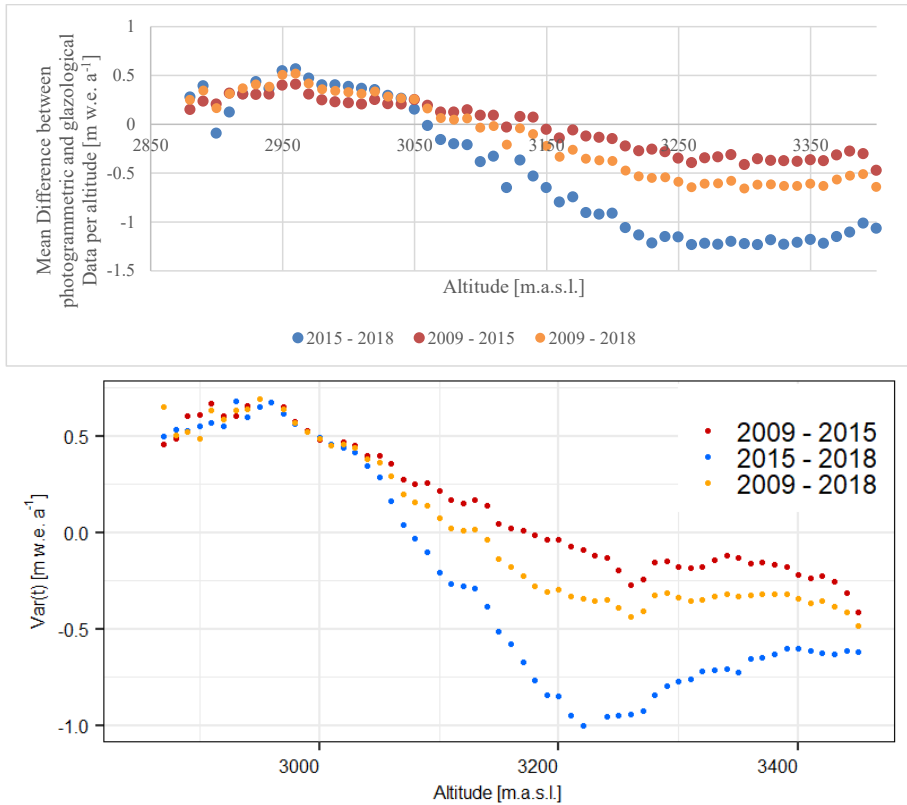
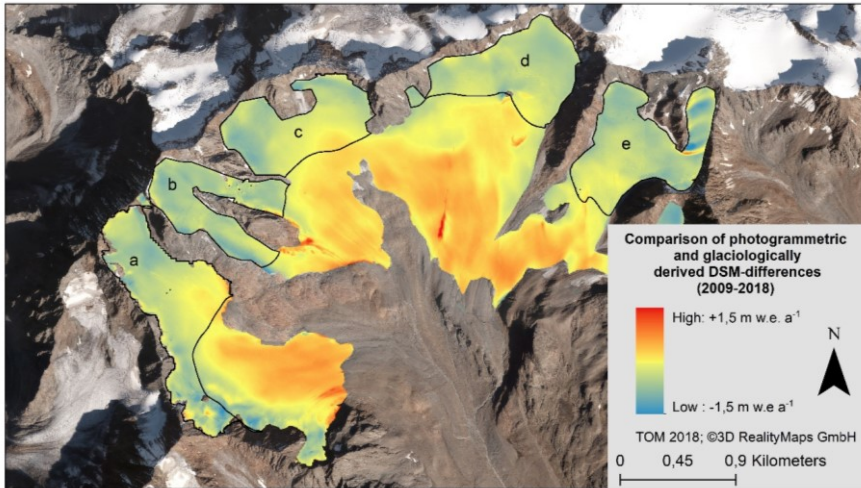


Figure 9: Comparison of photogrammetric DSM differences and glaciologically derived mass balances, depending on the altitude [m w.e. a⁻¹] after the correction of acquisition dates for all periods t; Positive values are present where $B_{glact} < B_{geod,t}$, negative values are present for the opposite relation, see Eq. 7.

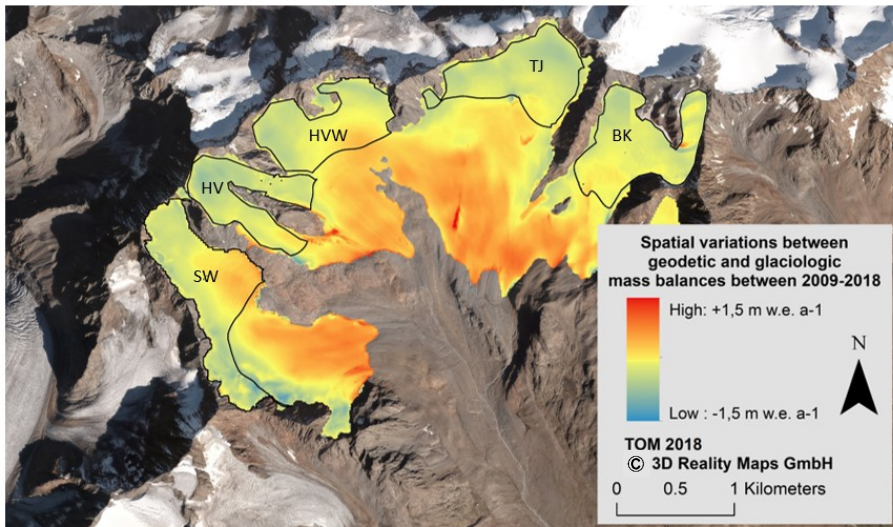
Assuming all deviations between photogrammetrically geodetic and glaciologically derived DSM differences mass balances (Fig. 9) are caused by dynamic processes, the magnitude of emergence and submergence is computed using the Variation Raster and Eq. 1 and 2. Between 2009 and 2018, the mean emergence (between 2900 m.a.s.l. and 3050 m.a.s.l.) is $0.34 \text{ m w.e. a}^{-1} \pm 0.25 \text{ m w.e. a}^{-1}$, with a maximum at most positive value being $0.527 \pm 0.25 \text{ m w.e. a}^{-1}$. Submergence occurs at altitudes higher than 3150 m.a.s.l. and results in a mean of $-0.48 \text{ m w.e. a}^{-1} \pm 0.25 \text{ m w.e. a}^{-1}$, with a maximum of $-0.65 \text{ m w.e. a}^{-1} \pm 0.25 \text{ m w.e. a}^{-1}$, with the most negative value being $-0.48 \pm 0.25 \text{ m w.e. a}^{-1}$ (Fig. 10). For a glacier in balance, the change between submergence and emergence regions occurs close to the equilibrium line. However, the mean ELA of the Vernagtferner is about 3250 m for the period 2009-2018 and thus roughly 150 m higher than the switch between apparent emergence and submergence.

When comparing the five different accumulation basins of the Vernagtferner shows that the mean differences are greater the derived submergence is more negative for higher basins with the largest offsets for the remaining true accumulation regions Hochvernagt, Broehkogel and Taschachhochjoch (Figure 10-).

hat formatiert: Nicht Hochgestellt/ Tiefgestellt



	Accumulation area	Mean submergence between 2009 and 2018 above 3150 m.a.s.l. [m w.e. a ⁻¹]	Area > 3150 m.a.s.l. [km ²]
a	Schwarzwand	-0,43	0,69
b	Hochvernagt	-0,59	0,44
c	Hochvernagt wand	-0,42	0,54
d	Taschachhochjoch	-0,48	0,56
e	Brochkogel	-0,52	0,62
	Vernagtferner	-0,48	2,85



	Accumulation Area	Mean submergence between 2009 and 2018 [m w.e. a ⁻¹]	Area > 3150 m.a.s.l. [km ²]	
	SW	Schwarzwand	- 0.26	0.69
	HV	Hochvernagt	- 0.38	0.44
	HVW	Hochvernagt wand	- 0.30	0.54
	TJ	Taschachhochjoch	- 0.41	0.56
	BK	Brochkogel	- 0.28	0.62
	VN	Vernagtferner (total)	- 0.32	2.85

450 **Figure 10: Top: Variation Raster 2015-2009-2018: Comparison of spatial variations of the corrected photogrammetric DSM differences and geodetic and glaciologically derived glaciologic mass balance data; Blue areas symbolize glaciologically derived DSM differences being higher than the photogrammetric DSM differences, with negative variations represent areas where $B_{geod.} < B_{glac.}$. In red areas, glaciologically obtained DSM differences are lower than the photogrammetric DSM differences, the opposite relation is present (see Eq. 7). For regions that appear yellow, both methods present similar height changes. Black outlines represent the different accumulation areas of the Vernagtferner; The mean submergence variation is given for each accumulation area in m w.e. a⁻¹, having an associated error of ± 0.25 m w.e.**

455

5.3 Other glaciers within the study site

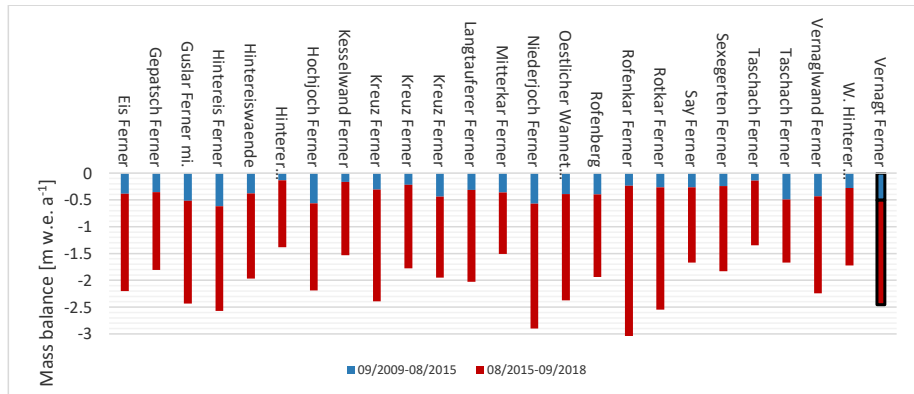
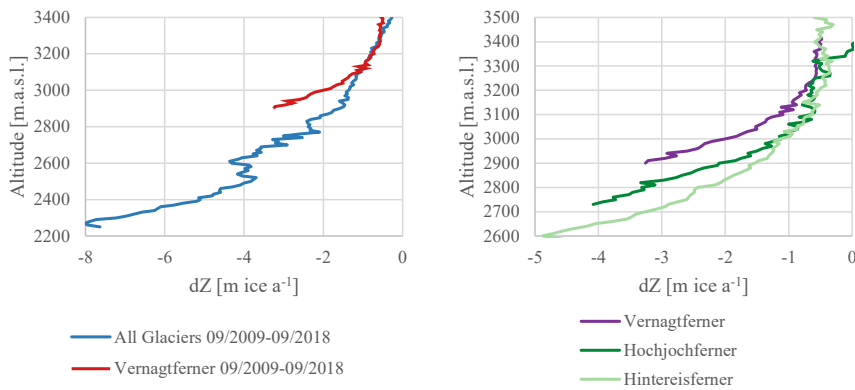
The major advantage of the photogrammetric mass balance assessment-geodetic mass balances compared to glaciological mass balances is that large areas can be investigated in great spatial detail. Therefore to highlight this benefit, we investigated the geodetic mass balance of all glaciers in the study area (sect. 4.1.2-). The mean height difference over the glacier surface was determined and converted into m w.e. as described above. The mean geodetic mass balance of all glaciers was -0.3846 ± 0.0506 m w.e. a⁻¹ for all glaciers 09/2009-08/2015, while it quadruples to -1.6459 ± 0.2221 m w.e. a⁻¹ between 08/2015 and 09/2018. For the whole period (09/2009-09/2018), the mean geodetic mass balance of all glaciers is -0.84 ± 0.11 m w.e. a⁻¹. It must be noted that there was no correction applied for the acquisition times. Accordingly, the mass balances do not refer to identical annual periods. However, if a time correction is assumed to have a similar influence on the annual mass balances of other

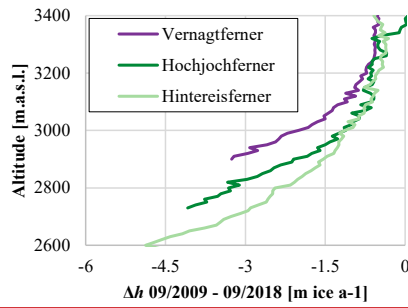
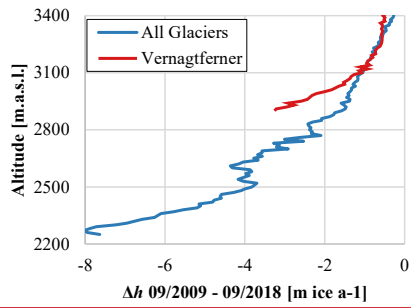
460

465

glaciers as it had for the Vernagtferner (-27% for 09/2009-08/2015 and +21% for 08/2015-09/2018,), the mean mass balances of all glaciers can be estimated. Accordingly, the mean annual glacier mass balance within the study area would be $-0.48 \pm 0.06 \text{ m w.e. a}^{-1}$ for the period 2009-2015 and $-1.26 \pm 0.06 \text{ m w.e. a}^{-1}$ for the period 2015-2018. The comparative values for the Vernagtferner exceed those values by 51% and 21%, respectively (). compares the altitude-related height losses of the Vernagtferner to the mean of all glaciers of the study area and the Hintereis- and Hochjochferner (and) glaciological data.

470





475

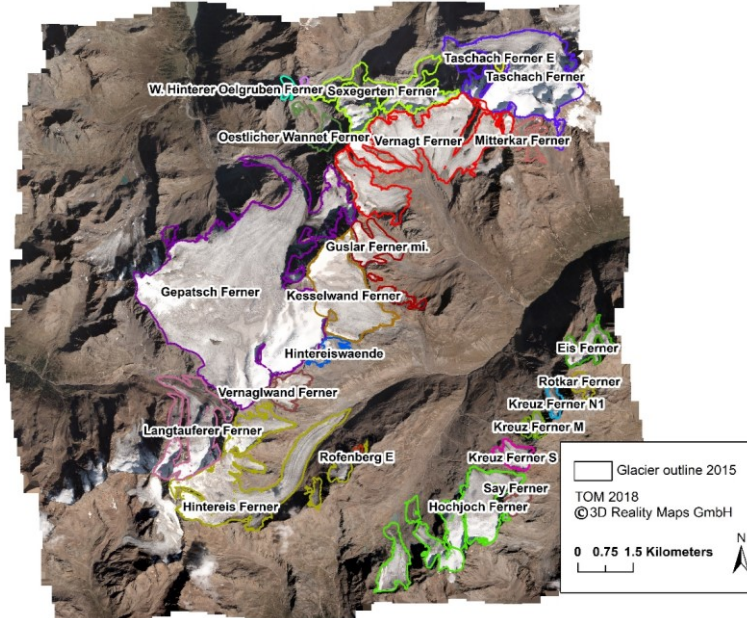
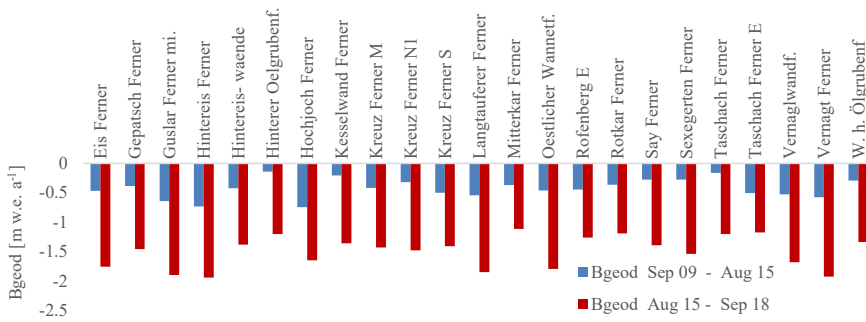


Figure 11: Annual height changes per altitude between 09/2009 and 09/2018 for the Vernagtferner compared to (i) all glaciers within the study area (top left) and (ii) to the Hochjochferner and Hintereisferner (top right); Comparison of all-glacier geodetic mass balances of all glaciers within the study area for the two investigation periods (middle)

If a time correction is assumed to have a similar influence on the annual mass balances of other glaciers as it had for the Vernagtferner (-34 % for 09/2009-08/2015, +20 % for 08/2015-09/2018, and +1.2 % for 09/2009-09/2018, Fig. 8), the mean mass balances of all glaciers can be estimated. Accordingly, the mean annual glacier mass balance within the study area would be -0.61 ± 0.07 m w.e. a^{-1} (2009-2015), -1.25 ± 0.14 m w.e. a^{-1} (2015-2018) and -0.83 ± 0.1 m w.e. a^{-1} (2009-2018). Thus, the geodetic mass balance of the Vernagtferner for the same periods is 25 %, 21 %, and 22 % more negative than the mean of all glaciers (Fig. 8).

6 Discussion

In this study, we investigated multitemporal changes in surface heights of selected glaciers in the Ötztal Alps with high spatial resolution. We derived geodetic mass balances for 23 glaciers within our study area and found that, for the Vernagtferner, glacier mass loss accelerated within the last decade. At the same time, the absolute surface height changes showed a maximum at low altitudes for all glaciers (Fig. 7). As it was shown for the Vernagtferner, peak volume loss occurs at higher altitudes, compared to the altitude where maximum surface height losses occur, since the volume is directly linked to the area-height-distribution of a glacier. These findings correspond to general observations (i) for the Vernagtferner (BADW, 2019; Escher-Vetter, 2015) and (ii) for most of the glaciers in the Alps. This study showed the great potential of using photogrammetry for glacier studies. Thus, height changes can easily be investigated for large areas with high spatial resolution and accuracy. As a result, for instance, we were able to estimate the decrease in length of the Hochjochferner ($826.4 \text{ m} \pm 0.2 \text{ m}$) between 09/2009 and 09/2018 and the maximum height changes at the glacier tongue of Hintereisferner, as shown in ($-20.4 \text{ m} \pm 0.4 \text{ m}$) with an accuracy of 0.2 m and 0.4 m respectively. A similar analysis and visualization could easily be applied to all the other glaciers within the study site. Furthermore, dead ice bodies can be mapped very well using the high-resolution photogrammetric data. For instance, on the north-facing side of the valley, below the glacier tongue of Hintereisferner, a large dead ice body is visible and ice loss could be determined for this feature, which is not included in the glaciological mass balance measurements. Another result derived from the DSM differences is and (ii) for most of the glaciers in the Alps (Fischer et al., 2015b; Fischer et al., 2015a; Huss, 2012). For instance, we derived a geodetic mass balance of -1.14 ± 0.02 m w.e. a^{-1} for the Hintereisferner (Table A1) for the period 09/2009 – 09/2018. The annual glaciologic mass balance for the same period, measured by the Institute of Atmospheric and Cryospheric Sciences of the University in Innsbruck, is -1.238 m w.e. a^{-1} (WGMS, 2020) and thus only 8% less negative.

We further evaluated the vertical surface height changes as a function of elevation (Fig. 7). Even though they cannot be compared to glaciologically derived vertical balance profiles directly, they illustrate (i) the relation of height losses to altitude and (ii) a shift between the two observation periods, the relation of height losses to altitude (Kaser et al., 2003; Pellikka and Rees, 2010). We found that the elevation change of all glaciers within our study site (i) is on average less negative compared to the Vernagtferner, (ii) is correlated to the altitude of the glacier tongue, and (iii) increased between 09/2009-08/2015 and 08/2015-09/2018 (Fig. 11). Besides glacier analysis, dead ice bodies can be mapped very well using high-resolution photogrammetric data. For instance, on the north-

facing side of the valley, below the glacier tongue of Hintereisferner, a dead ice body is visible. The volume change of this dead ice body (Fig. 4) was determined for the period 2009 – 2018: $(5.7 \pm 0.98) * 10^6 \text{ m}^3$.

Moreover, the comparison of the uncorrected photogrammetric total mass balances reveals the great potential of photogrammetry for glacier analysis. A large number of glaciers may be analyzed with a high spatial resolution and for the exact same time. For the Ötztaler Alps, based only on the photogrammetric DSM differences, we found that the elevation change (i) is on average lower compared to the Vernagtferner, (ii) is correlated to the altitude of the glacier tongue and (iii) increased between 09/2009–08/2015 and 08/2015–09/2018 (-).

The error assessment conducted reveals the high precision of the photogrammetric data with ~~SD~~the SD of the vertical error not exceeding 0.42 m for all DSM differences (Fig. 6). Moreover, the variation of the vertical error is normally distributed. A relation was found for the vertical error regarding the aspect, which is presumably based on the ~~vertical~~horizontal shift of the DSM (see sect.4.1.1). ~~The error caused by the~~This relation to the aspect can cause a larger error than the value we suggest, especially for glaciers with homogeneous orientations. By applying a full coregistration, following Nuth and Kääb (2011), this rotational error could have been addressed. Nevertheless, the 95% confidence interval used in this study covers most of these variations. (Fig. 6). ~~Future studies, that want to deduct this error, may follow the methodology suggested by-~~

Semivariograms determined ~~in order~~to assess the error for averaged values prove that this assumption was possible, since semivariance approximates a clear sill (further information on the method can be found in Rolstad et al., (2009)).

We used the density assumption of Huss (2013) to convert height changes to water equivalent. ~~It must be noted that~~The DSM differences 09/2009–09/2018 and 09/2009–08/2015 fulfill this assumption's prerequisites. This is not the case for the DSM difference 08/2015 – 09/2018 does not fulfill the prerequisite for this assumption, being a period shorter than three years. However, since the accumulation area ratio at ~~the~~Thus, the density assumption for this period must be considered with caution. For the Vernagtferner is relatively small, the density, we applied a novel density function based on the known altitude of the lost volume will be close ELA. The presented density function is transferable to other glaciers once the density-elevation of the ELA is known. Since the ELA can be estimated from geodetic surveys (Vargo et al., 2017), the presented density function is also suitable for future research on glaciers for which no glaciological data are available. We recommend, however, adjusting the density values of ice (900 kg/m^3), this seems and firn to be a good assumption ~~the corresponding region~~.

~~To~~We developed a robust methodology to adjust photogrammetricgeodetic mass balances to the acquisition time of the glaciologic measurements (30 September 30th), a correction was applied. An additional UAV survey was conducted, which made it possible to assess allowed assessing vertical height changes during the last one month of the ablation period in 2018 (Fig. 3). Therefrom, a regression function (sigmoid) was determined to correct estimate surface changes relative to the offsets of the acquisition dates in 2009, 2015, elevation. We incorporated meteorological data from a nearby climate station by using PDD for all relevant periods and 2018. The correctionelevation bins. Our regression function includes an uncertainty for the accumulation areas since the UAV survey did not cover the entire glacier area. Additionally, the intra-annual variation of melting and snowfall introduces another unknown, but important, source of error. More precisely, the transfer of the correction function from September 2018 to another year (here September 2009 and 2015) is strongly dependent on the meteorological conditions of the specific period. For instance, a snowfall event shortly before the survey would introduce an unknown error. The retrospective correction of the time periods therefore is not more than an approximation to

560 However, we showed that the presented workflow provides good results as they agree well with glaciological values. This uncertainty must be taken into account, in particular for the shorter observation periods 2009–2015 and 2015–2018, where the correction has a higher impact (–). This might explain that the deviations to the glaciological data increase for shorter periods mass balances (Fig. 8). Thus, we focused our analysis of the submergence on the period 2009–2018, where the impact of correction is lowest (–).

565 For transferability to other glaciers, individual correction functions from UAV surveys must be determined for each glacier, as these are directly related to glacier-specific slope gradients, orientation, the height of the glacier tongue, and area-height distributions (Fig. 11). Additional UAV surveys, which are low-cost and more flexible, but cover smaller areas, may be conducted to determine could enable the retrospective correction of recent geodetic mass balance data and improve the comparison with glaciologic mass balances. However, our method will perform best if the accumulation area ratio and area-height distribution remain similar between the period to be corrected and the period of the determined correction function of any glacier within the study site. This allows the adjustment of the respective DSM difference. Thus, the retrospective correction is limited to glaciological periods and therefore a comparison with the magnitudes of the glaciological data few years only. Best results can be expected if the UAV survey, thus the correction function represents the ablation processes, is conducted in the same season as the period that needs corrections. If the correction function is applied to photogrammetric mass balances retrospectively, intra-annual variation must be considered. In that case, if a more detailed analysis of the annual variations is needed, a mass balance model would produce more reliable results corrected.

575 Despite the above-mentioned potential causes of errors, we showed that the presented workflow to correct the photogrammetric elevation changes to full multi-annual mass balances provides good results. These results agree well with the glaciological mass balances (–), but show characteristic deviations in the elevation distribution (–). Thus, they are (i) suitable for detecting systematic errors in the glaciological method (–) and (ii) the method is transferable to other glaciers. This result is of great importance for future studies. Large-area, cadastral aerial surveys are usually recorded at any time in autumn and are therefore useless for verification of glaciological measurements.

585 For our case, the Vernagtferner, comparing Comparing the corrected photogrammetrically derived DSM differences geodetic with interpolated glaciologic mass balance rasters from glaciological measurements, revealed small-scale differences as well as general offsets due to ice dynamics (–). Such local deviations usually (Fig. 10). They mainly occur in highly crevassed areas, in and debris-covered areas, due to temporal changes in the snowpack and thus agree with findings of other studies (Fischer, 2011; Pellikka and Rees, 2010). They originate in the lack of glaciologic ablation stakes that are not located in such areas, and thus the glaciologic method interpolates within the accumulation area, internal and basal melting and interpolation errors of the glaciological method those regions. For crevassed areas, the deviations found at the Vernagtferner are negligible. With regard to Regarding the influence of debris cover (about 3.8 % of the total glacier surface) on the glacier mass balance, the effect results to 0.8 ± 0.6 % of the annual total for the period 2009–2018, we found that glaciologic mass balance, which is not represented by the spatial interpolation of the glaciological measurements at the moment would be 7.7 % less negative if such regions would be considered within interpolation. Debris-cover might play an increasing role when debris-covered glacier areas increase due to further glacier decline (Scherler et al., 2018). This could increase increases the need to conduct high-resolution geodetic observations in addition to glaciological measurements because point measurements on debris-covered parts are not always representative.

hat formatiert: Hervorheben

Surprisingly, the differences between geodetic and glaciological volume change in the accumulation areas do not reveal large spatial deviations, even though the glaciological results rely on very sparse in situ data. This demonstrates that the long-term accumulation conditions at Vernagtferner, which are known from former detailed investigations (Mayer et al., 2013a; Mayer et al., 2013b), are spatially relatively stable and can be used for scaling

600 the point measurements. ~~Even though~~However, this comparison of geodetic and glaciological results in the accumulation region has the potential to improve the representation of spatial variability across these areas.

~~Assuming that internal and basal melting are~~The deviations between the geodetic and glaciologic mass balances also showed a clear dependency on the elevation (Fig. 9) for all periods. These deviations are constant for the ablation areas for all periods but vary for the accumulation areas by a factor of three. We assumed that internal and basal melting is negligible, and the influence of temporal snowpack differences is small due to the long period of investigation and the rather small ratio of accumulation area. We thus interpret the remaining differences result from variations as the large-scale dynamic processes: submergence and emergence. They become quantifiable when looking at the mean differences/variations per altitude of both methods (Fig. 9), whereby the high spatial resolution and accuracy is absolutely crucial, and 10). It is noticeable that the observed switch between emergence and submergence (Fig. 9) is about 100 ~~to 150~~ m below the ELA of the Vernagtferner ~~for the respective period 2009-2018~~ (BAW, 2019) and roughly 200 m below the ELA for the period 2015-2018. While the ELA increased between the two periods (2009—2015 vs. 2015—2018) by about 60 m, the change from submergence to emergence decreased by about ~~90~~30 m. The reasons for this development are unknown but might indicate a further deviation from balanced conditions during recent years. ~~Even though the derived submergence is depending on the correction function, the values for the Vernagtferner and its accumulation areas correspond to literature values and~~The derived submergence must be considered with high caution since it is neither validated with field measurements nor model results. Presented submergence values are also based on i) our applied correction with sparse data for the accumulation region, ii) on the interpolation of a few glaciologic stake readings, and iii) our assumption that internal and basal processes are negligible. Those values (Fig. 10) are thus error-prone and should

610 only be referred to as a rough estimation. However, they show differences between the individual accumulation areas, which support glaciological observations (Lambrecht et al., 2011; Mayer et al., 2013b).
Future aerial image acquisitions aiming at calculating glacier mass balances must be as close as possible to each other (same date within the year) and preferably at the end of the ablation season. Ideally, these acquisitions are taken close to the standard glaciological mass balance data of 30 September ~~30th~~, to allow a direct comparison with available field information. ~~It should be ensured that the survey covers the entire surface of the glacier.~~ Since aerial image surveys require cloud-free weather, it will not always be possible to acquire the images on this exact date. ~~For this reason, temporal corrections, as successfully implemented within this study, will play an essential role in future studies. Additionally, future photogrammetric data acquisitions should be as large as possible, but at least cover the entire glacier area.~~

625 ~~For future research in the presented field, we see great potential in reanalyzing glacier mass balances using existing aerial imagery.~~ Since the late 2000s, European state surveying agencies have been carrying out cadastral surveys every two to four years with digital sensors and horizontal overlap of 80%, thus creating an immense multitemporal database of aerial imagery suitable for such purposes. The scientific and commercial consideration of those imageries would allow a three-dimensional reconstruction, mapping, and multitemporal analysis of vast areas in

635 the Alps with a resolution in the order of decimetres. This paper presented a robust method to account for the
resulting differences in acquisition dates and to project geodetic mass balances to full glaciologic periods.

7 Conclusion

This study demonstrates the high-potential of aerial images and the resulting ~~DSM's~~DSM's for analyzing glacier
retreat in great spatial and temporal detail. For all 2523 glaciers within the study area, height changesgeodetic mass
640 balances were analyzedderived with a 20 cm0.2 m spatial resolution and compared to each other. It was shown
that the glacier retreat does not only take place in low altitudes, but that even high accumulation basins are
meanwhile affected due to non-compensated ice flow. The altitudeelevation of the most significanthighest glacier
height changes, as well as and the amount of maximum volume loss, has have increased within our observation
period. If all aerial surveys that are available for large parts of the Alps were used, the majority of all alpine glaciers
645 could be analyzed by the presented method in the future. The spatial resolution of the respective analysis would
be significantly higherbetter than in other recent satellite-based studies. TheWe compared the photogrammetric
results were compared-with glaciological in-situ measurements. The required correction of acquisition dates was
successfully applied by using an additional UAV survey. This showsWe showed that the main disadvantage of
using photogrammetry, not being able to survey at the right timetime of glaciologic mass balance acquisition, can
650 be reduced by using additionalcomplementary UAV surveys, which can be better targeted in time. This study also
shows that results from the glaciological method can be greatly complemented with photogrammetric analyses,
which increasesincreasing the accuracy of the glaciological mass balance series, revealsrevealing regions of
anomalous mass balance conditions, and allowsallowing estimates of the imbalance between mass balance and ice
dynamics.

8 Appendices

Appendix A

Name	Δh_k	Δh_k	Δh_k	B_{geod}	B_{geod}	B_{geod}	Area	Area	Area
	09/2009	08/2015	09/2009	09/2009	08/2015	09/2009			
	-	-	-	-	-	-	2009	2015	2018
	08/2015	09/2018	09/2018	08/2015	09/2018	09/2018	[km ²]	[km ²]	[km ²]
	[m]	[m]	[m]	[m w.e. a ⁻¹]	[m w.e. a ⁻¹]	[m w.e. a ⁻¹]			
Eis Ferner	-3.285	-6.199	-9.484	-0.465	-1.756	-0.896	0.836	0.773	0.628
Gepatsch Ferner	-2.717	-5.149	-7.866	-0.385	-1.459	-0.743	18.951	18.775	18.589
Guslar Ferner mi.	-4.535	-6.709	-11.243	-0.642	-1.901	-1.062	1.556	1.415	1.268
Hintereis Ferner	-5.175	-6.850	-12.025	-0.733	-1.941	-1.136	7.127	6.440	6.101
Hintereiswaende	-2.977	-4.879	-7.856	-0.422	-1.382	-0.742	0.414	0.414	0.338
Hinterer Oelgruben Ferner	-0.999	-4.234	-5.232	-0.141	-1.200	-0.494	0.058	0.058	0.053
Hochjochferner	-5.261	-5.813	-11.075	-0.745	-1.647	-1.046	4.901	4.340	3.841
Kesselwandferner	-1.443	-4.806	-6.249	-0.204	-1.362	-0.590	3.697	3.597	3.563
Kreuz Ferner M	-2.967	-5.050	-8.017	-0.420	-1.431	-0.757	0.343	0.329	0.180
Kreuz Ferner N1	-2.252	-5.231	-7.483	-0.319	-1.482	-0.707	0.273	0.252	0.205
Kreuz Ferner S	-3.534	-4.965	-8.499	-0.501	-1.407	-0.803	0.559	0.531	0.456
Langtaufenerferner	-3.836	-6.524	-10.360	-0.543	-1.849	-0.978	3.069	3.043	2.886
Mitterkar Ferner	-2.612	-3.930	-6.542	-0.370	-1.113	-0.618	0.536	0.536	0.515

<u>Östlicher Wannetferner</u>	<u>-3.249</u>	<u>-6.332</u>	<u>-9.581</u>	<u>-0.460</u>	<u>-1.794</u>	<u>-0.905</u>	<u>0.582</u>	<u>0.582</u>	<u>0.419</u>
<u>Rofenberg E</u>	<u>-3.154</u>	<u>-4.463</u>	<u>-7.616</u>	<u>-0.447</u>	<u>-1.264</u>	<u>-0.719</u>	<u>0.089</u>	<u>0.085</u>	<u>0.067</u>
<u>Rotkar Ferner</u>	<u>-2.552</u>	<u>-4.201</u>	<u>-6.753</u>	<u>-0.362</u>	<u>-1.190</u>	<u>-0.638</u>	<u>0.224</u>	<u>0.224</u>	<u>0.108</u>
<u>Say Ferner</u>	<u>-1.949</u>	<u>-4.909</u>	<u>-6.858</u>	<u>-0.276</u>	<u>-1.391</u>	<u>-0.648</u>	<u>0.270</u>	<u>0.270</u>	<u>0.252</u>
<u>Sexegertenferner</u>	<u>-1.962</u>	<u>-5.429</u>	<u>-7.391</u>	<u>-0.278</u>	<u>-1.538</u>	<u>-0.698</u>	<u>2.980</u>	<u>2.905</u>	<u>2.462</u>
<u>Taschachferner</u>	<u>-1.143</u>	<u>-4.241</u>	<u>-5.384</u>	<u>-0.162</u>	<u>-1.202</u>	<u>-0.508</u>	<u>5.818</u>	<u>5.779</u>	<u>5.302</u>
<u>Taschach F. E</u>	<u>-3.570</u>	<u>-4.153</u>	<u>-7.723</u>	<u>-0.506</u>	<u>-1.177</u>	<u>-0.729</u>	<u>0.049</u>	<u>0.049</u>	<u>0.049</u>
<u>Vernaglwandferner</u>	<u>-3.718</u>	<u>-5.941</u>	<u>-9.659</u>	<u>-0.527</u>	<u>-1.683</u>	<u>-0.912</u>	<u>0.745</u>	<u>0.700</u>	<u>0.576</u>
<u>Vernagtferner</u>	<u>-4.048</u>	<u>-6.802</u>	<u>-10.849</u>	<u>-0.573</u>	<u>-1.927</u>	<u>-1.025</u>	<u>7.327</u>	<u>7.015</u>	<u>6.096</u>
<u>W. H. Oelgrubenf.</u>	<u>-2.068</u>	<u>-4.724</u>	<u>-6.792</u>	<u>-0.293</u>	<u>-1.339</u>	<u>-0.641</u>	<u>0.143</u>	<u>0.143</u>	<u>0.128</u>

Table A1: Surface changes [m] and geodetic mass balance [m w.e.] of all glaciers within the study area.

hat formatiert: Schriftart: Kursiv

660 *Data availability.* Except for the aerial imagery and derived products, all datasets are available on request. Geodetic mass balance data will be submitted to WGMS.

Author contributions. Conceptualization, Methodology, Investigation, Formal Analysis and Writing – Original Draft, JG; Validation, CM; Photogrammetric data acquisition and processing, JJ and FS; Glaciologic data acquisition and processing, CM; Writing – Review & Editing, JG, CM, FS, UM and JJ; Funding Acquisition, FS and UM; Supervision, CM, JJ, FS. All authors have read and approved ~~of~~ the submitted version.

Competing interests. The authors declare that they have no conflicts of interest.

670 *Acknowledgments.* We thank the Landesvermessungsamt Tirol for providing some of the aerial imagery.

Financial Support. This work was conducted as a part of the AlpSenseBench Project (2018-2019) funded by the Bavarian Ministry of Economic Affairs, Regional Development, and Energy.

89 References

- 675 Abermann, J., Lambrecht, A., Fischer, A. and Kuhn, M.: Quantifying changes and trends in glacier area and volume in the Austrian Ötztal Alps (1969-1997-2006), *The Cryosphere*, 3, 205–215, <https://doi.org/10.5194/tc-3-205-2009>, 2009.
- Auer, I., Böhm, R., Jurkovic, A., Lipa, W., Orlik, A., Potzmann, R., Schöner, W., Ungersböck, M., Matulla, C., Briffa, K., Jones, P., Efthymiadis, D., Brunetti, M., Nanni, T., Maugeri, M., Mercalli, L., Mestre, O.,
- 680 Moisselin, J.-M., Begert, M., Müller-Westermeier, G., Kveton, V., Bochnicek, O., Stastny, P., Lapin, M., Szalai, S., Szentimrey, T., Cegnar, T., Dolinar, M., Gajic-Capka, M., Zaninovic, K., Majstorovic, Z. and Nieplova, E.: HISTALP—historical instrumental climatological surface time series of the Greater Alpine Region, *Int. J. Climatol.*, 27, 17–46, <https://doi.org/10.1002/joc.1377>, 2007.
- Baltsavias, E. P., Favey, E., Bauder, A., Bösch, H. and Pateraki, M.: Digital Surface Modelling by Airborne
- 685 Laser Scanning and Digital Photogrammetry For Glacier Monitoring, *Photogrammetric Record*, 17(98): 243-273, available at: <http://www.mpateraki.org/wp-content/uploads/2014/11/ucl.pdf>, 2001.

- Belart, J. M. C., Magnússon, E., Berthier, E., Pálsson, F., Adalgeirsdóttir, G. and Jóhannesson, T.: The geodetic mass balance of Eyjafjallajökull ice cap for 1945–2014: processing guidelines and relation to climate, 0022-1430, <https://doi.org/10.1017/jog.2019.16>, 2019.
- 690 Beniston, M., Farinotti, D., Stoffel, M., Andreassen, L. M., Coppola, E., Eckert, N., Fantini, A., Giacona, F., Hauck, C., Huss, M., Huwald, H., Lehning, M., López-Moreno, J.-I., Magnusson, J., Marty, C., Morán-Tejéda, E., Morin, S., Naaim, M., Provenzale, A., Rabatel, A., Six, D., Stötter, J., Strasser, U., Terzago, S. and Vincent, C.: The European mountain cryosphere: a review of its current state, trends, and future challenges, *The Cryosphere*, 12, 759–794, <https://doi.org/10.5194/tc-12-759-2018>, 2018.
- 695 Braithwaite, R. J. and Zhang, Y.: Sensitivity of mass balance of five Swiss glaciers to temperature changes assessed by tuning a degree-day model, *Journal of Glaciology*, 46, 7–14, <https://doi.org/10.3189/172756500781833511>, 2000.
- Cogley, G.: Mass-balance terms revisited, *Journal of Glaciology*, 56, 997–1001, <https://doi.org/10.3189/002214311796406040>, 2010.
- 700 Cogley, G., Hock, R., Rasmussen, L. A., Arendt, A. A. and Zemp, M.: Glossary of glacier mass balance and related terms, 86, <https://doi.org/10.5167/uzh-53475>, 2011.
- Escher-Vetter, H.: 400 Jahre Feldforschung am Vernagtferner (Ötztal, Österreich), Lozan, J. L.; Graßl, H.; Kasang, D.; Notz, D.; Escher-Vetter, H. (5 editors) / Warnsignal Klima / Wissenschaftliche Auswertungen, Hamburg, 299pp, ch. 4.7 (146-154), 2015.
- 705 Escher-Vetter, H., Kuhn, M. and Weber, M.: Four decades of winter mass balance of Vernagtferner and Hintereisferner, Austria: methodology and results, *Annals of Glaciology*, 50, 87–95, <https://doi.org/10.3189/172756409787769672>, 2009.
- Fischer, A.: Comparison of direct and geodetic mass balances on a multi-annual time scale, *The Cryosphere*, 5, 107–124, <https://doi.org/10.5194/tc-5-107-2011>, 2011.
- 710 Fischer, A., Seiser, B., Stocker Waldhuber, M., Mitterer, C. and Abermann, J.: Tracing glacier changes in Austria from the Little Ice Age to the present using a lidar-based high-resolution glacier inventory in Austria, *The Cryosphere*, 9, 753–766, <https://doi.org/10.5194/tc-9-753-2015>, 2015a.
- Fischer, M., Huss, M. and Hoelzle, M.: Surface elevation and mass changes of all Swiss glaciers 1980–2010, *The Cryosphere*, 9, 525–540, <https://doi.org/10.5194/tc-9-525-2015>, 2015b.
- 715 Fliri, F.: *Das Klima im Raume von Tirol, Innsbruck-München*, 1975.
- Gobiet, A., Kotlarski, S., Beniston, M., Heinrich, G., Rajczak, J. and Stoffel, M.: 21st century climate change in the European Alps - a review, *The Science of the total environment*, 493, 1138–1151, <https://doi.org/10.1016/j.scitotenv.2013.07.050>, 2014.
- Hanzer, F., Förster, K., Nemeč, J. and Strasser, U.: Projected cryospheric and hydrological impacts of 21st century climate change in the Ötztal Alps (Austria) simulated using a physically based approach, *Hydrology and Earth System Sciences*, 22, 1593-1614, <https://doi.org/10.15488/3378>, 2018.
- 720 Heipke, C.: *Photogrammetrie und Fernerkundung*, Springer, Berlin, Heidelberg, Germany, 2017.
- Hirschmüller, H.: *Semi-Global Matching. Motivation, Developments and Applications*, available at: <https://elib.dlr.de/73119/1/180Hirschmueller.pdf>, 2019.
- 725 Hock, R.: Temperature index melt modelling in mountain areas, *Journal of Hydrology*, 282, 104–115, [https://doi.org/10.1016/S0022-1694\(03\)00257-9](https://doi.org/10.1016/S0022-1694(03)00257-9), 2003.

- Huss, M.: Extrapolating glacier mass balance to the mountain-range scale: the European Alps 1900–2100, *The Cryosphere*, 6, 713–727, <https://doi.org/10.5194/tc-6-713-2012>, 2012.
- Huss, M.: Density assumptions for converting geodetic glacier volume change to mass change, *The Cryosphere*, 7, 877–887, <https://doi.org/10.5194/tc-7-877-2013>, 2013.
- 730 Jaenicke, J., Mayer, C., Scharer, K., Münzer, U. and Gudmundsson, A.: The use of remote-sensing data for mass-balance studies at Mýrdalsjökull ice cap, Iceland, *Journal of Glaciology*, 52, 565–573, <https://doi.org/10.3189/172756506781828340>, 2006.
- Klug, C., Bollmann, E., Galos, S. Peter, Nicholson, L., Prinz, R., Rieg, L., Sailer, R., Stötter, J. and Kaser, G.: Geodetic reanalysis of annual glaciological mass balances (2001–2011) of Hintereisferner, Austria, *The Cryosphere*, 12, 833–849, <https://doi.org/10.5194/tc-12-833-2018>, 2018.
- 735 Lambrecht, A., Mayer, C., Hagg, W., Popovnin, V., Rezapkin, A., Lomidze, N. and Svanadze, D.: A comparison of glacier melt on debris-covered glaciers in the northern and southern Caucasus, *The Cryosphere*, 5, 525–538, <https://doi.org/10.5194/tc-5-525-2011>, 2011.
- 740 Magnússon, E., Muñoz-Cobo Belart, J., Pálsson, F., Ágústsson, H. and Crochet, P.: Geodetic mass balance record with rigorous uncertainty estimates deduced from aerial photographs and lidar data – Case study from Drangajökull ice cap, NW Iceland, *The Cryosphere*, 10, 159–177, <https://doi.org/10.5194/tc-10-159-2016>, 2016.
- Marty, C. and Meister, R.: Long-term snow and weather observations at Weissfluhjoch and its relation to other high-altitude observatories in the Alps, *Theor Appl Climatol*, 110, 573–583, <https://doi.org/10.1007/s00704-012-0584-3>, 2012.
- Mass balance of the Vernagtferner, AT: <https://geo.badw.de/vernagtferner-digital/massenbilanz.html>, last access: 19 July 2019.
- Mayer, C., Escher-Vetter, H. and Weber, M.: 46 Jahre glaziologische Massenbilanz des Vernagtferners, *Zeitschrift für Gletscherkunde und Glazialgeologie*, 45/46, 219–234, 2013a.
- 750 Mayer, C., Jaenicke, J., Lambrecht, A., Braun, L., Völksen, C., Minet, C. and Münzer, U.: Local surface mass-balance reconstruction from a tephra layer – a case study on the northern slope of Mýrdalsjökull, Iceland, *Journal of Glaciology*, 63, 79–87, <https://doi.org/10.1017/jog.2016.119>, 2017.
- Mayer, C., Lambrecht, A., Blumthaler, U. and Eisen, O.: Vermessung und Eisdynamik des Vernagtferners, *Ötztaler Alpen, Zeitschrift für Gletscherkunde und Glazialgeologie*, 45/46, 259–280, 2013b.
- 755 Nuth, C. and Kääb, A.: Co-registration and bias corrections of satellite elevation data sets for quantifying glacier thickness change, *The Cryosphere*, 5, 271–290, <https://doi.org/10.5194/tc-5-271-2011>, 2011.
- Östrem, G.: Ice Melting under a Thin Layer of Moraine, and the Existence of Ice Cores in Moraine Ridges, *Geografiska Annaler*, 228–230, <https://doi.org/10.1080/20014422.1959.11907953>, 1959.
- 760 Pellikka, P. K. E. and Rees, W. G. (Eds.): Remote sensing of glaciers: techniques for topographic, spatial and thematic mapping of glaciers, Taylor & Francis, New York, USA, 2010.
- Rogora, M., Frate, L., Carranza, M. L., Freppaz, M., Stanisci, A., Bertani, I., Bottarin, R., Brambilla, A., Canullo, R., Carbognani, M., Cerrato, C., Chelli, S., Cremonese, E., Cutini, M., Di Musciano, M., Erschbamer, B., Godone, D., Iocchi, M., Isabellon, M., Magnani, A., Mazzola, L., Di Morra Cella, U., Pauli, H., Petey, M., Petriccione, B., Porro, F., Psenner, R., Rossetti, G., Scotti, A., Sommaruga, R., Tappeiner, U., Theurillat, J.-P., Tomaselli, M., Viglietti, D., Viterbi, R., Vittoz, P., Winkler, M. and Matteucci, G.:

Assessment of climate change effects on mountain ecosystems through a cross-site analysis in the Alps and Apennines, *Science of The Total Environment*, 624, 1429–1442, <https://doi.org/10.1016/j.scitotenv.2017.12.155>, 2018.

770 Rolstad, C., Haug, T. and Denby, B.: Spatially integrated geodetic glacier mass balance and its uncertainty based on geostatistical analysis: application to the western Svartisen ice cap, Norway, *J. Glaciol.*, 55, 666–680, <https://doi.org/10.3189/002214309789470950>, 2009.

Scherler, D., Wulf, H. and Gorelick, N.: Global Assessment of Supraglacial Debris-Cover Extents, *Geophys. Res. Lett.*, 45, 798–805, <https://doi.org/10.1029/2018GL080158>, 2018.

775 Sommer, C., Malz, P., Seehaus, T. C., Lippl, S., Zemp, M. and Braun, M.: Rapid glacier retreat and downwasting throughout the European Alps in the early 21 st century, *Nat Commun*, 11, 1–10, <https://doi.org/10.1038/s41467-020-16818-0>, 2020.

Vargo, L. J., Anderson, B. M., Horgan, H. J., Mackintosh, A. N., Lorrey, A. M. and Thornton, M.: Using structure from motion photogrammetry to measure past glacier changes from historic aerial photographs, *Journal of Glaciology*, 63, 1105–1118, <https://doi.org/10.1017/jog.2017.79>, 2017.

780 WGMS: Global Glacier Change Bulletin, available at: https://wgms.ch/products_ref_glaciers/hinterisferner-alps/, 2020.

Zekollari, H., Huss, M. and Farinotti, D.: Modelling the future evolution of glaciers in the European Alps under the EURO-CORDEX RCM ensemble, *The Cryosphere*, 13, 1125–1146, <https://doi.org/10.5194/tc-13-1125-2019>, 2019.

785 Zemp, M., Thibert, E., Huss, M., Stumm, D., Rolstad Denby, C., Nuth, C., Nussbaumer, S. U., Moholdt, G., Mercer, A., Mayer, C., Joerg, P. C., Jansson, P., Hynek, B., Fischer, A., Escher-Vetter, H., Elvehøy, H. and Andreassen, L. M.: Reanalysing glacier mass balance measurement series, *The Cryosphere*, 7, 1227–1245, <https://doi.org/10.5194/tc-7-1227-2013>, 2013.

790